Continental sedimentary processes decouple Nd and Hf isotopes

Marion Garçon, Catherine Chauvel, Christian France-Lanord, Pascale Huyghe, Jérôme Lavé

Elsevier Editorial System(tm) for Geochimica et Cosmochimica Acta
Manuscript Draft

Manuscript Number: GCA-D-12-00845R1

Title: Continental sedimentary processes decouple Nd and Hf isotopes

Article Type: Article

Corresponding Author: Dr. Marion Garçon, Ph.D

Corresponding Author's Institution: ISTerre

First Author: Marion Garçon, PhD

Order of Authors: Marion Garçon, PhD; Catherine Chauvel; Christian France-Lanord; Pascale Huyghe; Jérôme Lavé

Abstract: The Nd and Hf isotopic compositions of most crustal and mantle rocks correlate to form the "Terrestrial Array". However, it is now well established that whereas coarse detrital sediments follow this trend, fine-grained oceanic sediments have high Hf ratios relative to their Nd isotopic ratios. It remains uncertain whether this "decoupling" of the two isotopic systems only occurs in the oceanic environment or if it is induced by sedimentary processes in continental settings. Here, we focus on the Hf and Nd isotopic compositions of sediments in large rivers in order to constrain the behavior of the two isotopic systems during erosion and sediment transport from continent to ocean.
We report major and trace element concentrations together with Nd and Hf isotopic compositions of bedloads, suspended loads and river banks from the Ganges River and its tributaries draining the Himalayan Range i.e. the Karnali, the Narayani, the Kosi and the Marsyandi Rivers. Our sample set includes sediments sampled within the Himalayan Range in Nepal, at the Himalayan mountain front, and also downstream on the floodplain and at the outflow of the Ganges in Bangladesh. We show that hydrodynamic sorting of minerals explains the entire Hf isotopic range, i.e. more than 10 εHf units, observed in the river sediments but does not affect the Nd isotopic composition. Bedloads and bank sediments have systematically lower εHf values than suspended loads sampled at the same location. Coarse-grained sediments lie below or on the Terrestrial Array in an εHf vs. εNd diagram. In contrast, fine-grained sediments, including most of the suspended loads, deviate from the Terrestrial Array toward higher εHf relative to their εNd, as is the case for oceanic terrigenous clays. We explain the observed Nd-Hf decoupling by mineralogical sorting processes that enrich bottom sediments in coarse and dense minerals, including unradiogenic zircons, while surface sediments are enriched in fine material with radiogenic Hf signatures. We demonstrate that Nd-Hf isotopic decoupling increases with sediment transport in the floodplain to reach its maximum at the river mouth. The Nd-Hf isotopic decoupling observed in worldwide oceanic clays and river sediments is likely to have the same origin. Finally, we estimated the Nd-Hf isotopic composition of the present-day mantle if oceanic sediments had never been subducted and conclude that the addition of oceanic sediments with their anomalous Nd-Hf isotopic compositions has slowly shifted the composition of the Earth's mantle towards more radiogenic Hf values.

Continental sedimentary processes decouple Nd and Hf isotopes

Marion Garçon[1], Catherine Chauvel[1], Christian France-Lanord[2], Pascale Huyghe[1], Jérôme Lavé[2]

[1] ISTerre, CNRS, Université Joseph Fourier de Grenoble, BP 53, 38041 Grenoble Cedex 09, France

[2] CRPG-CNRS, Vandoeuvre lès Nancy, France

Corresponding author:
Marion Garçon
marion.garcon@ujf-grenoble.fr
+33 4 76 51 40 63

Abstract

The Nd and Hf isotopic compositions of most crustal and mantle rocks correlate to form the "Terrestrial Array". However, it is now well established that whereas coarse detrital sediments follow this trend, fine-grained oceanic sediments have high Hf ratios relative to their Nd isotopic ratios. It remains uncertain whether this "decoupling" of the two isotopic systems only occurs in the oceanic environment or if it is induced by sedimentary processes in continental settings. Here, we focus on the Hf and Nd isotopic compositions of sediments in large rivers in order to constrain the behavior of the two isotopic systems during erosion and sediment transport from continent to ocean.

We report major and trace element concentrations together with Nd and Hf isotopic compositions of bedloads, suspended loads and river banks from the Ganges River and its tributaries draining the Himalayan Range i.e. the Karnali, the Narayani, the Kosi and the Marsyandi Rivers. Our sample set includes sediments sampled within the Himalayan Range in Nepal, at the Himalayan mountain front, and also downstream on the floodplain and at the outflow of the Ganges in Bangladesh. We show that hydrodynamic sorting of minerals explains the entire Hf isotopic range, i.e. more than 10 ε_{Hf} units, observed in the river sediments but does not affect the Nd isotopic composition. Bedloads and bank sediments have systematically lower ε_{Hf} values than suspended loads sampled at the same location. Coarse-grained sediments lie below or on the Terrestrial Array in an ε_{Hf} vs. ε_{Nd} diagram. In contrast, fine-grained sediments, including most of the suspended loads, deviate from the Terrestrial Array toward higher ε_{Hf} relative to their ε_{Nd}, as is the case for oceanic terrigenous clays. We explain the observed Nd-Hf decoupling by mineralogical sorting processes that enrich bottom sediments in coarse and dense minerals, including unradiogenic zircons, while surface sediments are

enriched in fine material with radiogenic Hf signatures. We demonstrate that Nd-Hf isotopic decoupling increases with sediment transport in the floodplain to reach its maximum at the river mouth. The Nd-Hf isotopic decoupling observed in worldwide oceanic clays and river sediments is likely to have the same origin. Finally, we estimated the Nd-Hf isotopic composition of the present-day mantle if oceanic sediments had never been subducted and conclude that the addition of oceanic sediments with their anomalous Nd-Hf isotopic compositions has slowly shifted the composition of the Earth's mantle towards more radiogenic Hf values.

Keywords: Nd, Hf, river sediments, decoupling of isotopic systems, mineralogical sorting

1. Introduction

The present-day Nd and Hf isotopic compositions of most crustal and mantle-derived rocks correlate and form the "Terrestrial Array" (Vervoort et al., 1999; Vervoort et al., 2011) due to similar fractionation of Sm/Nd and Lu/Hf during magmatic processes. However, it is also recognized that some oceanic sediments, in particular oceanic ferromanganese crusts and terrigenous clays, deviate significantly from the Terrestrial Array towards higher ε_{Hf} values relative to their ε_{Nd} values (e.g. Albarède et al., 1998; Vervoort et al., 1999; van de Flierdt et al., 2004; Chauvel et al., 2008; Bayon et al., 2009; Vervoort et al., 2011). The exact cause of this shift in Nd-Hf isotopic compositions is still debated (e.g. Bau and Koschinsky, 2006; van de Flierdt et al., 2007; Vervoort et al., 2011). Patchett et al. (1984), Chauvel et al. (2008), Carpentier et al. (2009) and Vervoort et al. (2011) suggest that the decoupling in terrigenous oceanic sediments is due to sequestration on continents of zircons with low ε_{Hf}: the so-called "zircon effect" e.g., a process that transports material with elevated Lu/Hf and Hf isotopic ratios to the ocean basins. Authors who mainly concentrated on seawater and ferromanganese crusts have more diverse interpretations. For example, Pettke et al. (2002) and Rickli et al. (2010) evaluated the input of eolian dusts with high ε_{Hf} values while Bayon et al. (2006), van de Flierdt et al. (2007), Bayon et al. (2009), Godfrey et al. (2009), Chen et al. (2011), Vervoort et al., (2011) and Rickli et al. (2013) suggested that the decoupling could be due to preferential release of radiogenic Hf during chemical weathering of phases with high Lu/Hf such as apatite.

Almost all studies suggest that the Nd and Hf isotopes are decoupled on continents and inherited by the oceanic sediments. However, only few studies have focused on continental sediments (e.g. Bayon et al., 2006; Rickli et al., 2013) and Nd-Hf isotopic systematics of river sediments have never been thoroughly investigated. A

proper understanding of these processes is required if Nd-Hf isotopes are to be used as provenance and weathering proxies and also, at a more global scale, to determine the Nd-Hf isotopic composition of the continental crust and mantle. We currently do not know whether zircon-rich sediments largely remain on the continents or are transported into ocean basins. In addition, if the composition of sediment recycled into the mantle in subduction zones differs from average continental crust, how does this decoupling of the two isotopic systems affect the long-term evolution of the mantle?

The aim of this paper is to accurately document the Nd-Hf isotopic compositions of sediments transported by large rivers to better understand the behavior of the two isotopic systems during erosion and sediment transport from land to sea. To accomplish this, we use a comprehensive sample set including bedloads, bank deposits and suspended loads at the Himalayan front and floodplain of the Ganges, Karnali, Narayani and Kosi Rivers, along the Marsyandi River in the Himalayan Range in Nepal, and at the mouths of small tributaries draining single geological units.

The Ganges River and its tributaries constitute one of the largest fluvial systems in the world (Lupker et al., 2011). The immense size of this fluvial network, together with its importance in the world sedimentation system, provide the opportunity to study global Nd-Hf isotopic systematics of river sediments. Sediments from the Ganges and its major tributaries have been widely studied, in particular (a) in provenance studies (Galy and France-Lanord, 2001; Garzanti et al., 2007; Tripathi et al., 2007; Singh et al., 2008; Singh, 2009; Singh, 2010), (b) to determine the effects of chemical weathering (Galy and France-Lanord, 1999; Lupker et al., 2012), (c) to characterize mineralogical variations associated to hydraulic sorting (Garzanti et al., 2010; Garzanti et al., 2011), (d) to quantify organic carbon transfer (Galy et al., 2007; Galy et al., 2008) and (e) to estimate global sediment flux budgets (Galy and France-Lanord, 2001; Lupker

et al., 2011). Using these studies and our new results, we investigated the effects of sediment provenance and mineral sorting during sediment transport on the trace-element concentrations and Nd-Hf isotopic compositions of these river sediments.

2. The Ganges fluvial system

The Ganges fluvial system is one of the main conveyors of material eroded from the Himalayan Range, delivering ca. 400 million tons of sediments per year (Lupker et al., 2011) to the ocean in the Bay of Bengal. Together with the Brahmaputra River, the Ganga ranks among the three largest fluvial systems in terms of annual sediment load delivered into the ocean (Milliman, 2001). The sediments accumulate in the Bengal fan, by far the largest fan in the world with its volume of 12.5×10^6 km^3 and a sediment mass of ca. 3×10^{16} tons (Curray, 1994; Curray et al., 2003).

The Ganges and its major tributaries drain an area of about 1 million km^2 that stretches over 2500 km from its sources in the High Himalayan Range to its delta in Bangladesh (Figure 1). The water discharge of the Ganges is strongly controlled by the monsoon from June to September, which accounts for about 75% of its annual flow in Bangladesh (Singh et al., 2007). The Ganges basin (Figure 1) includes several major tributaries, the Yamuna, Karnali, Narayani and Kosi Rivers, which drain the southern flank of the Himalayan Range in the north and the Chambal River, which drains part of the Indian shield and the Deccan Traps basalts in the south. Le Fort (1975) divided the Ganges drainage basin in the Himalayan Range, into four geological units: (1) the Tethyan Sedimentary Series, which consists of weakly metamorphosed Cambrian to Eocene carbonates and clastic sedimentary rocks (dark grey in Figure 1); (2) the High Himalayan Crystalline units mostly composed of strongly metamorphosed Neoproterozoic to Ordovician gneiss, migmatites, and marbles (light grey in Figure 1);

(3) the Lesser Himalaya units of weakly metamorphosed Proterozoic sedimentary rocks (white in Figure 1); and (4) the Neogene to Quaternary Siwalik molasses which are floodplain deposits of recycled erosion products from the Himalayan Range (orange in Figure 1). France-Lanord et al. (1993) and Galy and France-Lanord (2001) showed that more than two thirds of the sediments transported by the Ganges River derived from the High Himalayan Crystalline units, with the remainder coming from the Lesser Himalaya units.

The mineralogy of Ganges sediments includes both inherited and neoformed mineral phases and is controlled by hydrodynamic processes during fluvial transport (see Galy et al., 2008; Garzanti et al., 2010; Garzanti et al., 2011). Supplementary Table A reports estimates of Garzanti et al. (2010, 2011) of the average mineral proportions of bedloads and suspended loads sampled in the Ganges in Bangladesh. According to these studies, bedloads contain higher proportions of quartz (40 to 60%) and heavy minerals (up to 15%) than suspended loads (27 to 55% quartz and 3 to 6% heavy minerals). Heavy minerals include amphibole, epidote, garnet and many accessories such as titanite, zircon, monazite, allanite, apatite and tourmaline (Supplementary Table A). By contrast, suspended load sediments tend to be enriched in phyllosilicates such as clays (8 to 26%) and micas (9 to 30%).

3. Sediment Sampling and analytical procedure

3.1. Sediment Sampling

River sediments analyzed in this study were sampled over several years of field campaigns, in Nepal, India and Bangladesh. Some of these samples have already been analyzed for major elements (Lupker et al., 2012), Re-Os isotopes (Pierson-Wickmann et

al., 2000), mineralogical proportions (Garzanti et al., 2007; 2010; 2011) and C_{org} isotopes (Galy et al., 2008).

To document the Nd-Hf isotopic variability of river sediments at a large scale, i.e. during their transport from the mountain range to the delta, we analyzed a set of samples from the Ganges and its major tributaries (Karnali, Narayani and Kosi Rivers) collected at the front of the Himalayan Range and in the floodplain (Figure 1). Because more than 95% of the suspended load is transported during the monsoon season (Islam et al., 1999), most samples were collected between July and September from 1993 to 2010. We also studied the isotopic variability of the sediments at a smaller scale using 10 samples collected in the Himalayas along the Marsyandi River, from its source at ca. 5000 m altitude to its confluence with the Trisuli River in Nepal at an altitude of ca. 250 m (pink star in Figure 1). The precise locations of these samples, together with a detailed description of the Marsyandi Basin, can be found in Attal and Lavé (2006) and Garzanti et al. (2007) while GPS derived coordinates are provided in Supplementary File B. Finally, we analyzed sediments from small Nepalese rivers draining monolithologic basins to characterize the chemical and isotopic compositions of the three main Himalayan geological units i.e. the Lesser Himalaya, the High Himalayan Crystalline and the Tethyan Sedimentary Series (white, light grey and dark grey stars in Figure 1).

To study the effects of mineralogical sorting on the eroded material transported by the Ganges, we analyzed different types of river sediment at each sampling site. Wherever possible, the suspended load was sampled at the surface and at different depths in the water column, and additional samples were obtained from dredged bedload sediments and bank sediments. Sampling techniques for suspended load, bedload and bank sediment are provided in Galy et al. (2008) and Lupker et al. (2011).

3.2. Chemical analyses

3.2.1. Major element contents

Major element contents were measured in the sediments from the Marsyandi River and from the Nepalese rivers draining single geological units. Major element concentrations in all the other studied samples were published by Lupker et al. (2012) (See Supplementary Table B). After freeze-drying and grinding with an agate mortar to ensure homogeneity, about 100 mg of sediments were fused using lithium metaborate to measure major element concentrations by ICP-AES at the SARM in Nancy (France) according to the technique described by Govindaraju and Mevelle (1987) and Carignan et al. (2007).

3.2.2. Trace element concentrations and Nd-Hf isotopes

3.2.2.a. Sample preparation and dissolution

The samples were further ground in agate bowls using a planetary ball mill to insure fine grain size. About 50 to 100 mg of powder were initially treated with 5 mL of 14N HNO_3 on a hotplate for 2 days. After evaporation, the samples were digested in a 10:1 mixture of 5 mL HF and 0.5 mL $HClO_4$ using teflon containers placed in steel PARR bombs for 6 weeks at 140°C or one week at 200°C. The digestion time and temperature needed to completely dissolve resistant minerals such as zircons were previously estimated by several tests comparing (1) the trace element content of river sediments (suspended load, bedload and bank deposit from the Ganges) being digested at different temperatures during 1, 3 and 6 weeks with (2) the trace element content of the same samples being fused with lithium metaborate, a technique that ensures total digestion of all resistant minerals. Such tests indicate that sediments must be digested during at least

6 weeks at 140°C or one week at 200°C to ensure total dissolution of zircons and other resistant minerals. After complete dissolution, two aliquots were taken from each sample: one to measure trace element concentrations and the other to isolate Nd and Hf for isotopic measurements.

3.2.2.b. Trace element concentrations

Trace element concentrations were measured using an Agilent 7500ce ICP-MS in Grenoble (France) following the procedure described by Chauvel et al. (2011). Measurements were performed on samples diluted 5000 times in a solution of 2% HNO_3 with traces of HF. They were corrected for oxide interference and ICP-MS analytical drift using a multispike of Be, Ge, In, Tm and Bi. Repeated measurements of BR or BR-24 rock standards were used as an external calibration to calculate trace element concentrations in all samples. The validity and the reproducibility of our results are assessed by repeated measurements of international rock standards as unknown samples, including sedimentary materials such as JSd-2, and the measurements of several complete duplicates (see Supplementary Tables B and C).

3.2.2.c. Nd-Hf isotopic compositions

Hf and Nd were isolated using ion chromatography (Chauvel et al., 2011). Total procedural blanks reached on average 94 pg (n=6) for Nd and 47 pg (n=11) for Hf and are negligible compared to the amount of Nd and Hf isolated in all samples (on average 1600 ng for Nd and 600 ng for Hf). Neodymium and Hf isotopic compositions were analyzed on a Nu Plasma HR MC-ICP-MS at the ENS Lyon (France) and were corrected for mass fractionation bias using $^{146}Nd/^{144}Nd=0.7219$ and $^{179}Hf/^{177}Hf=0.7325$,

respectively. The average measured values for the Ames-Rennes Nd and Ames-Grenoble Hf reference standards run every two or three samples are $^{143}Nd/^{144}Nd$ = 0.511959 ± 8 (2σ, n = 59) and $^{176}Hf/^{177}Hf$ = 0.282163 ± 10 (2σ, n = 99), respectively. MC-ICP-MS analytical drift was corrected using the recommended values for these two standards ($^{143}Nd/^{144}Nd$ = 0.511961 ± 13; Chauvel and Blichert-Toft (2001) and $^{176}Hf/^{177}Hf$ = 0.282160 ± 12; Chauvel et al. (2011)). The reproducibility of our results estimated using complete duplicate analyses is usually better than 0.5 ε units for Nd and Hf isotopic compositions (see Table 1).

4. Results

4.1. Major and Trace element concentrations

Major element contents are presented in Supplementary Table B. For the purpose of this study, we focus on the SiO_2 and Al_2O_3 contents of the studied bedloads, bank deposits and suspended loads, as shown in Figure 2a. Lupker et al. (2011, 2012) describe the variations of other major elements. In general, SiO_2 and Al_2O_3 contents are strongly correlated with sediment grain-size (Lupker et al., 2011). Bedloads and bank sediments are enriched in coarse-grained quartz and have high SiO_2 contents (ca. 70-80 wt.%), and relatively low Al_2O_3 (ca. 5-12 wt.%), Fe_2O_3 (ca. 2-5 wt.%), K_2O (ca. 1-3 wt.%), MgO (ca. 1-3 wt.%) and TiO_2 (ca. 0.1-0.6 wt.%). Suspended loads have lower SiO_2 (ca. 50-70 wt.%) and tend to have higher contents of elements hosted by fine phyllosilicates such as Al_2O_3 (ca. 10-18 wt.%), Fe_2O_3 (ca. 4-8 wt.%), K_2O (ca. 3-5 wt.%), MgO (ca. 2-5 wt.%) and TiO_2 (ca. 0.5-1 wt.%). Due to this chemical differentiation, Al_2O_3/SiO_2 ratios can be used as a reliable grain-size proxy for detrital sediments: Figure 2b shows that bedloads and bank deposits have lower Al_2O_3/SiO_2 ratios than suspended loads. Moreover, Lupker et al.

279 (2011) showed that Al_2O_3/SiO_2 ratios of suspended loads are very well correlated with
280 their sampling depth in the water column. This feature, not shown in Figure 2, accounts
281 for the variability of Al_2O_3/SiO_2 ratios in suspended loads: surface suspended loads have
282 higher Al_2O_3/SiO_2 ratios than those sampled at greater depths. It can also be seen in
283 Figure 2 that some of the bedloads and bank deposits have surprisingly high Al_2O_3/SiO_2
284 ratios. These samples were recovered during the dry season when weak water flow
285 favored deposition of Al_2O_3-rich phyllosilicates in bedloads and bank sediments.

286 Trace-element concentrations are presented in the Supplementary Table B.
287 Spidergrams normalized to the average upper continental crust composition of Rudnick
288 and Gao (2003) are shown in Figure 3 for sediments from the Nepalese rivers draining
289 exclusively the Tethyan Sedimentary Series, the High Himalayan Crystalline and the
290 Lesser Himalaya units (Figure 3a-c) and for the Marsyandi, Ganges, Narayani, Karnali
291 and Kosi Rivers (Figure 3d-h).

292 In the Himalayan Range, sediments from small Nepalese rivers draining single
293 sources display variable trace element distributions (Figure 3a-c). They are
294 systematically depleted in transition elements and mobile elements such as Ba and Sr.
295 Enrichment factors are generally higher for the Tethyan Sedimentary Series than for the
296 High Himalayan Crystalline and the Lesser Himalaya units. The trace-element
297 characteristics can be quantified using element concentrations and ratios normalized to
298 the average upper continental crust (e.g. $(Th/U)_{UCC}$). Sediments from Tethyan
299 Sedimentary Series show clear enrichments in Cs, Rb, Li and As, very high $(Th/U)_{UCC}$
300 ratios (2.0±0.6 (1σ) on average) and rather flat REE patterns (average $(La/Yb)_{UCC}$ of
301 1.2±0.3 (1σ)). By contrast, the REE patterns of sediments eroded from High Himalayan
302 Crystalline units are characterized by significant enrichments in heavy REE (average

303 $(La/Yb)_{UCC}$ of 0.4±0.2 (1σ)). Lesser Himalaya sediments show much more variability
304 with $(La/Yb)_{UCC}$ ratios ranging from 0.7 to 1.4.

305 Trace-element concentrations measured in sediments collected along the high-
306 altitude Marsyandi river are more variable than those sampled in rivers on the
307 floodplain (see Figure 3d-h). When compared to the average upper continental crust
308 composition, most are enriched in Cs, Rb and depleted in Ba, Sr and transition elements
309 (Sc, V, Cr, Co, Ni, Cu, Zn and As). Enrichment factors for Zr-Hf range from 0.3 to 1.5 and
310 from 0.8 to 4.4 for Th-U. Their REE patterns display a small enrichment in heavy REE, as
311 shown by their average $(La/Yb)_{UCC}$ ratio of 0.7±0.3 (1σ).

312 In the floodplain, trace-element patterns for sediments from the Ganges and its
313 major tributaries draining the Himalayan Range i.e. the Narayani, the Karnali and the
314 Kosi Rivers resemble each other (Figure 3e-h). No systematic downstream variation in
315 their composition occurs and trace-element distributions are globally comparable to the
316 composition of average upper continental crust, except for the transition elements and
317 some mobile elements (Ba, Sr) which are always depleted. REE patterns are generally
318 flat with an average $(La/Yb)_{UCC}$ ratio of 0.8±0.1 (1σ) for the Ganges sediments, 0.9±0.1
319 (1σ) for the Narayani sediments, 0.9±0.2 (1σ) for the Karnali sediments and 0.9±0.1 (1σ)
320 for the Kosi sediments. There is no significant REE fractionation between bedload,
321 suspended load and bank deposits (average $(La/Yb)_{UCC}$ of 0.9±0.2 (1σ) for all of the
322 bedloads and bank sediments and 0.9±0.1 (1σ) for all of the suspended loads). In
323 general, bedloads and bank sediments are characterized by a positive anomaly in Zr-Hf
324 and are more depleted than suspended loads in transition elements and mobile
325 elements such as Cs, Rb and Ba. In the Ganges River, bedloads and bank sediments show
326 significant enrichments in all REE and positive Th-U anomalies (Figure 3e). These

features are not observed in the Narayani, the Karnali and the Kosi Rivers for which the chemical compositions of bedloads, bank deposits and suspended loads are similar.

4.2. Nd-Hf isotopic compositions

Neodymium and Hf isotopic compositions measured in this study are given in Table 1. Sediments sampled in the Himalayan Range from rivers draining single geological units and from the Marsyandi River are shown in a ε_{Hf} vs. ε_{Nd} diagram in Figure 4 together with worldwide isotopic compositions of oceanic sediments. Sediments from the floodplain of the Ganges and its major tributaries are shown in Figure 5.

In the Himalayan Range (Figure 4), Nd-Hf isotopes of sediments from the Lesser Himalaya units display significantly less radiogenic values ($-40.3 < \varepsilon_{Hf} < -28.8$ and $-25.1 < \varepsilon_{Nd} < -20.1$) than those from the High Himalayan Crystalline units ($-22.2 < \varepsilon_{Hf} < -12.7$ and $-17.7 < \varepsilon_{Nd} < -12.9$) and the Tethyan Sedimentary Series ($-23.7 < \varepsilon_{Hf} < -19.5$ and $-18.3 < \varepsilon_{Nd} < -16.6$). The ε_{Nd} values are comparable to Nd isotopic compositions published for bedrocks from the Lesser Himalaya, the High Himalayan Crystalline and the Tethyan Sedimentary Series (see the histogram in Figure 4 and references therein).

Neodymium and Hf isotopic compositions of bedloads sampled all along the Marsyandi River (Figure 4) are much less variable ($-25.5 < \varepsilon_{Hf} < -19.9$ and $-18.0 < \varepsilon_{Nd} < -15.4$) and resemble those of the High Himalayan Crystalline and the Tethyan Sedimentary Series. There is no clear downstream variation in ε_{Hf} and ε_{Nd} values (see Figure 6; Table 1).

In the floodplain (Figure 5), Nd-Hf isotopic compositions of sediments from the Ganges River and its major tributaries are similar. The Hf isotopic compositions are nevertheless more variable ($-30.2 < \varepsilon_{Hf} < -18.3$) than Nd isotopes ($-20.1 < \varepsilon_{Nd} < -15.6$).

With the exception of few outliers, bedloads and bank sediments tend to lie below or on the Terrestrial array while suspended loads, which have higher ε_{Hf} values, usually plot above the array with compositions approaching those of worldwide oceanic terrigenous clays. By contrast, suspended loads, bedloads and bank deposits cannot be distinguished using their Nd isotopic compositions.

5. Discussion

5.1. Source isotopic variability

The Nd and Hf isotopic compositions of sediments along a river course are influenced by contributions of materials with different isotopic compositions that are supplied by tributaries. These source effects need to be evaluated before we can consider any other control on the geochemistry of river sediments.

REE barely fractionate during weathering and have been widely used for studying the provenance of detrital sediments. More specifically, ratios such as La/Yb, or Nd isotopic compositions of weathered material, are considered to represent the compositions of source rocks (Goldstein and Jacobsen, 1988; Condie, 1991; Taylor and McLennan, 1995). We evaluate below how these proxies vary in the Himalayan river sediments.

5.1.1. The Marsyandi River in the Himalayan Range

In the Himalayan Range, the Marsyandi River has its source at ca. 5000m altitude in the Tethyan Sedimentary Series, then flows down through High Himalayan Crystalline and Lesser Himalaya units to the floodplain at ca. 250 m altitude (Figure 6). Samples recovered upstream, where the river drains only the Tethyan Sedimentary Series

(samples NAG 22 and MAR-50), are characterized by an average $(La/Yb)_{UCC}$ ratio of 1.2±0.3 (1σ) and a ε_{Nd} value of -16.8±0.3 (1σ) (Table 1).

Downstream, when the river passes through the High Himalayan Crystalline units (samples MAR-55 and MAR-58), the average $(La/Yb)_{UCC}$ ratio drops to 0.7±0.4 (1σ) while average ε_{Nd} values are comparable to values obtained upstream (ε_{Nd} = -16.2±0.1 (1σ)). The REE patterns of sediments are thus clearly affected by materials eroded from the High Himalayan Crystalline units, which have an average $(La/Yb)_{UCC}$ ratio of 0.4±0.2 (1σ) (see section 4.1). Because the Nd isotopic signature of the Tethyan Sedimentary Series is similar to that of the High Himalayan Crystalline units (see the histogram in Figure 4 and references therein), there is no significant change in the average ε_{Nd} values of the sediments.

Farther downstream, sediments sampled where the river passes through the Lesser Himalaya units (all MAR samples downstream of MAR-58) are characterized by an average $(La/Yb)_{UCC}$ ratio of 0.6±0.3 (1σ) and an ε_{Nd} value of -16.7±1.1 (1σ). This value is remarkably similar to that measured upstream even though the Lesser Himalaya units have a significantly less radiogenic Nd isotopic signature (see the histogram in Figure 4 and references therein). This shows that the Lesser Himalaya units contribute little to the final sediment load of the Marsyandi River, as already suggested by Garzanti et al. (2007). Using petrographic and mineralogical data, Garzanti et al. (2007) suggest contributions of 13±5%, 68±3% and 20±2% from the Tethyan Sedimentary Series, the High Himalayan Crystalline and the Lesser Himalayan units, respectively. Assuming comparable Nd concentrations for sediments from the three main sources, our mixing calculations show that addition of 20% Lesser Himalayan sediments with an ε_{Nd} of -23.2, to sediments derived from the other two sources ($\varepsilon_{Nd} \approx$ -16.5) only lowers the isotopic composition of the mixture by 1.3 ε_{Nd} unit, a value consistent with our measurements.

In summary, despite the fact that the Marsyandi River crosses several geological units with distinct isotopic signatures ($-25<\varepsilon_{Nd}<-13$), its sediments have rather constant ε_{Nd} values of -16.6±2.1 (1σ) on average. The variability of Nd isotopic compositions due to source effects is limited (i.e. about 3 ε_{Nd} units) and the sediments are effectively homogenized within the Himalayan Range before they enter the floodplain.

5.1.2. The Ganges and its major tributaries in the floodplain

Floodplain sediments of the Ganges and its major tributaries have remarkably similar REE patterns with an average $(La/Yb)_{UCC}$ ratio of 0.88 (see section 4.1. and Figure 3). As shown in Figure 5, their Nd isotopic compositions span a small range of values (less than 5 ε_{Nd} units) similar to values obtained for the bedrocks from the High Himalayan Crystalline units and the Tethyan Sedimentary Series (Figure 4). Nor is there any systematic change in REE patterns and Nd isotopic compositions of river sediments sampled at the Himalayan mountain front and farther downstream in the floodplain. This indicates that no significant amount of new material is added along the course of the Ganges, as already suggested in earlier studies using major and trace elements (Tripathi et al., 2007; Singh et al., 2008; Singh, 2009; Lupker et al., 2012).

Sediments derived from erosion of the Indian shield and the Deccan Traps are also added to the Ganges (see Figure 1) and one might expect that these terranes could influence the Nd isotopic composition of sediments after their confluence. However, Lupker et al. (2012) excluded significant contributions from these sources and estimated the contribution of the southern tributaries to the entire Ganges sediment load to be less than 4% in Bangladesh when our samples were recovered in 2004, 2007 and 2008. Our new ε_{Nd} values support this interpretation in that sediments collected in Bangladesh have values similar to upstream samples.

Within the range of ε_{Nd} values obtained for the floodplain samples (-20 to -15), the most negative values are likely due to higher contributions of sediments from the Lesser Himalaya units depending on the sampling period and/or location. This could notably be the case for the Kosi and Narayani sediments (green and purple dots in Figure 5). For example, the ε_{Nd} values of the Narayani samples, which were all collected at the same location in Nepal, vary from -19.5 to -17.3 depending on sampling time (July 2005, August 2007 and July 2010). This suggests that part of the Nd isotopic variability in Figure 5 could be temporal and related to inefficient local homogenization of the sediments due to changes of the river flow conditions throughout the hydrological cycle or from a year to the other. Such a phenomenon was already advocated by Lupker et al. (2012) for Ganges sediments sampled in Bangladesh and by Viers et al. (2008) for the Amazon River.

5.2. Effects of hydrodynamic sorting of minerals

Sediments transported by rivers consist of particles and minerals with different hydrodynamic properties that depend on their size, shape and density but are independent of their primary or secondary origin. This results in "mineral sorting" within the water column: coarse and dense grains are preferentially transported in bedload by sliding and bouncing while fine and light grains are preferentially transported in suspended load and at different depth in the water column depending on their settling velocities. The most common coarse and dense grains usually consist of minerals resistant to weathering processes such as quartz, zircon or monazite. In contrast, the light and fine grains in the suspended load include primary mineral phases such as mica as well as secondary minerals formed during weathering (clays). Because chemical elements are present in different concentrations in minerals, mineral sorting

produces significant geochemical variability in river sediments (Singh and France-Lanord, 2002; Garzanti et al., 2010; Bouchez et al., 2011; Garzanti et al., 2011; Lupker et al., 2011). To assess its impact on the Nd-Hf isotopic systematics of the Himalayan river sediments, we first briefly describe its influence on major and trace element concentrations, then focus on the Nd and Hf budgets.

5.2.1. Impact on the overall chemical compositions

The influence of mineral sorting during sediment transport on the major and trace element concentrations of sediments from the Himalayan rivers was studied in detail by Garzanti et al. (2010, 2011) and Lupker et al. (2011, 2012). Our new measurements are consistent with results obtained by these authors. As the factor controlling the Al_2O_3 and SiO_2 contents is sediment grain size (Lupker et al., 2011), Al_2O_3/SiO_2 ratio can be used as a reliable grain-size proxy: coarse-grained sediments i.e. most of the bedloads and bank deposits, are enriched in SiO_2-rich quartz while finer-grained sediments, i.e. most of the suspended load, are enriched in Al_2O_3-rich phyllosilicates (see Figure 2).

Systematic changes of trace-element concentrations between bedloads, bank sediments and suspended loads also occur (Figure 3). Suspended loads generally have higher concentrations of transition and mobile elements due to their high proportion of phyllosilicates, oxyhydroxides, soil particles and organic matter (Garzanti et al., 2011). For the other trace elements, differences between bedload, bank sediment and suspended load are more difficult to explain because they result from the combined effects of several processes: (1) contribution of mineral phases such as zircon, rutile or monazite that strongly control the budget of Zr-Hf, Nb-Ta and REE, respectively (Garçon et al., 2011); (2) the proportions of mineral species that occur in different quantities in

476 bedloads, banks and suspended loads; and (3) dilution by minerals such as quartz that
477 are relatively poor in trace elements. The combination of the three processes explains
478 why the trace element patterns of bedloads and bank sediments are not systematically
479 different from those of suspended loads in Figures 3f-g-h even though it is clear that the
480 two types of sediments do not share similar mineralogical compositions (cf.
481 Supplementary Table A and Garzanti et al., 2010; 2011). Bedloads and bank sediments
482 from the Ganges River are the only ones with trace-element patterns distinct from the
483 suspended loads (Figure 3e). As most Ganges sediments were sampled in the
484 Bangladesh delta, where river hydrodynamics are relatively calm, segregation of
485 minerals within the water column is more efficient and the difference between heavy
486 mineral-rich bedloads and clay-rich suspended loads is clearer than in sediments
487 sampled upstream in the floodplain.

488 Heavy minerals play a key role in the chemical budget of sediments because they
489 host specific elements in extreme concentrations: this is the case of Zr and Hf in zircon
490 and LREE, Th and U in monazite and allanite (e.g. Götze and Lewis, 1994; Totten, 2007;
491 Garçon et al., 2011). Along the Marsyandi River, Garzanti et al. (2007) show that the
492 proportion of heavy minerals in bank sediments is highly variable, ranging between 1
493 and 31 wt.% in the 63-250 μm fraction. We thus suggest that in the Marsyandi bank
494 sediments, highly variable proportions of heavy minerals are responsible for the large
495 variability of trace element contents (Figure 3d). Unfortunately, we cannot establish a
496 direct link between the heavy mineral proportions estimated by Garzanti et al. (2007)
497 and our trace element data because only four of our samples were analyzed by Garzanti
498 et al. (2007), and because the heavy mineral proportions determined by these authors
499 were not obtained on bulk samples but on the 63-250 μm fraction.

In the floodplain sediments, Zr-Hf anomalies are good proxies to the relative proportion of zircon and REE-bearing minerals. Most bedloads and bank sediments from the Ganges and its major tributaries exhibit a positive Zr-Hf anomaly, suggesting excess zircons, as is to be expected in coarse-grained sediments. However, the absence of positive Zr-Hf anomalies in most suspended loads and in some bedloads and bank sediments from the Narayani and Kosi Rivers does not imply that these sediments lack zircon; it simply means that the relative proportion of zircon to REE-bearing minerals is lower. Indeed, Garzanti et al. (2010, 2011) demonstrated that zircon controls almost the entire Zr-Hf budget of the Ganges bedloads and about half the Zr-Hf budget of surface suspended loads. They also demonstrated that monazite and allanite control the entire REE budget, including that of Nd in the Ganges bedloads, whereas phyllosilicates, together with titanite and monazite, are the carriers of REE in suspended loads. Our new trace element data further support this interpretation.

5.2.2. Nd-Hf isotopic decoupling

As discussed in section 5.2.1, Nd and Hf in bedloads and suspended loads are carried by different minerals whose proportions in the two types of sediments are controlled by sorting during transport. Since these minerals do not all have the same Sm/Nd and Lu/Hf ratios and formed millions of years ago, the Nd and Hf isotopic compositions of bedloads and suspended loads should differ.

Figures 4 and 5, where ε_{Hf} is plotted as a function of ε_{Nd}, show that bedloads and bank sediments plot on or slightly below the Terrestrial Array while suspended loads plot above. Figure 7 plots ε_{Nd} and ε_{Hf} as a function of Al_2O_3/SiO_2 i.e. the grain size proxy. No clear change of ε_{Nd} occurs as a function of the sediment grain-size, but the ε_{Hf} of coarse-grained sediments with low Al_2O_3/SiO_2 ratios are systematically lower than those

525 of fine-grained sediments with high Al_2O_3/SiO_2 ratios. This is particularly true when the
526 bedloads and bank sediments were sampled at the same location as the suspended loads
527 (see the color bands linking related samples in Figure 7). Given that source variability is
528 limited in these sediments (see section 5.1), our observations suggest that mineral
529 sorting during transport has a significant effect on Hf isotopic compositions but does not
530 change the Nd isotopic signature. Nd and Hf isotopes are thus decoupled in fine-grained
531 sediments with high Al_2O_3/SiO_2 ratios. This is confirmed by the remarkable correlation
532 between $\Delta\varepsilon_{Hf}$, a measure of the vertical ε_{Hf} deviation from the Terrestrial Array, and
533 Al_2O_3/SiO_2, as shown in Figure 8. With few exceptions, coarse-grained sediments lie
534 below or on the Terrestrial Array while $\Delta\varepsilon_{Hf}$ increases as grain size decreases in all other
535 sediments. We conclude that the entire Hf isotopic variability observed in the Himalayan
536 river sediments (more than 10 ε_{Hf} units) relates to changes in sediment grain size, and is
537 therefore due to mineral sorting during sediment transport.

538 Similar decoupling of Nd and Hf isotopes by mineral sorting has already been
539 reported in detrital oceanic materials (see Figure 4 and 5; Patchett et al., 1984; Chauvel
540 et al., 2008; Bayon et al., 2009; Carpentier et al., 2009; Vervoort et al., 2011) but, to our
541 knowledge, it has never before been demonstrated for modern river sediments on
542 continents. We believe that in both environments, sample mineralogy controls the
543 fractionation of Hf from Nd isotopes as described by Patchett et al. (1984). Zircon hosts
544 most of the Hf in river sediment and has very low Lu/Hf ratios (see Kinny and Maas,
545 2003 for a review) compared to any other mineral. Its Hf isotopic composition is
546 therefore very close to the initial ratio of the material from which it crystallized, and
547 always significantly less radiogenic than the Hf isotopic composition of all other crustal
548 minerals. Because coarse-grained sediments are zircon-rich, they inherit the
549 unradiogenic Hf isotopic composition of zircon. By contrast, the Hf isotopic composition

of fine-grained sediment varies depending on the relative proportion of zircon to other, more radiogenic minerals with high Lu/Hf ratios. These minerals include primary minerals formed during crystallization of the source rocks (i.e. muscovite, biotite) and secondary minerals formed through alteration and weathering (i.e. clays). Hence, we do not exclude that additional fractionation is introduced during differential chemical weathering of minerals with high Lu/Hf as suggested by several authors (Bayon et al., 2006; Godfrey et al., 2009; Chen et al., 2011; Vervoort et al., 2011, Rickli et al., 2013). Of course, the amplitude of the Hf isotopic fractionation also depends on the age of the crustal protolith since time is necessary to produce ^{176}Hf as a decay product of ^{176}Lu.

In contrast to Hf isotopes, mineral sorting appears to have minimal effect on Nd isotopes because the minerals that host Nd in bedloads, suspended loads and bank sediments (i.e. phyllosilicates, monazite, etc) have the same Sm/Nd ratio as their protolith. As a consequence, all sediments have the same Nd isotopic composition i.e. that of their source rocks. We demonstrated that this is clearly not the case for the Hf isotopic composition of sediments which strongly depends on the sample mineralogy; most sediments do not have the same Hf isotopic signature as their source rocks. Only coarse-grained sediments, rich in zircons, have Hf isotopes that can be used to estimate the composition of their continental sources provided that the age of the zircon population is known (Harrison et al., 2005; Kemp et al., 2007; Garçon et al., 2011).

5.3. Where does decoupling of Nd and Hf isotopes occur on continents?

Mineral sorting processes depend strongly on river hydrodynamics. Thus, the chemical and isotopic compositions of river sediments should vary as a function of sampling site, and values in the steep Himalayan Range should differ from those in the

floodplain. The extent of Nd-Hf isotopic decoupling in fine-grained sediments should also vary depending on the degree of mineral sorting.

In the Himalayan Range, ε_{Nd} values in the Marsyandi sediments vary within a small range between -18.0 and -15.4 (Figure 6) and are not significantly affected by source effects or mineralogical sorting. The same applies to ε_{Hf} values of bedloads, even though they are more variable (-25.5 to -19.9). The ε_{Hf} variability does not correlate with the Nd isotopic compositions of sediments, and is not related to the geological units through which the river flows (Figure 6). Because the modern river system does not contain long-term storage sites (Attal and Lavé, 2006), the data suggests that the Hf isotopic composition of the Marsyandi bedloads is controlled by local changes in the river hydrodynamics that influence the proportions of heavy minerals (see section 5.2.1. and Garzanti et al., 2007). We could not measure the isotopic compositions of suspended loads in the Marsyandi River and we cannot discuss how different they are from the bedloads. However, our bedload data alone suggest that the Hf isotopic variability of sediments sampled in the mountain range is mainly controlled by local hydrodynamic conditions.

The situation is very different, however, on the Ganges floodplain. Figure 9 shows the variations of Nd and Hf isotopic compositions of bedloads, suspended loads and bank sediments from the Ganges and its major tributaries as a function of sample locations. While ε_{Nd} values are remarkably constant at about -17.6 ± 1 (1σ) and do not change downstream, ε_{Hf} values display significant variations. As mentioned above, the Hf isotopic compositions of bedloads and bank sediments are less radiogenic than those of suspended loads sampled at the same location. Figure 9 shows clearly that this difference increases with distance from river source. This is particularly clear for Ganges sediments in which the Hf isotopic variation is less than 5 ε_{Hf} units near the border of the

600 Himalayas but reaches 12 ε_{Hf} units in the Bangladesh delta. Decoupling of Nd-Hf isotopes
601 exists at the front of the mountain range but becomes much more pronounced at the
602 river mouth. The increasing decoupling could result of enhanced differential chemical
603 weathering in the floodplain, with enhanced release of radiogenic Hf from high Lu-Hf
604 minerals in suspended loads. However, we do not observe any significant correlation
605 between ε_{Hf} values of suspended loads in the floodplain and the ratios used by Lupker et
606 al. (2012) to evaluate chemical weathering intensity (e.g. Na/Si, K/Si). Additionally, ε_{Hf}
607 values do not vary as a function of Lu/Hf or Ca/K from mountain front to delta, as would
608 be expected if radiogenic Hf were preferentially released by chemical weathering of high
609 Lu/Hf minerals (Bayon et al., 2006; Rickli et al., 2013). We therefore suggest that the
610 increasing decoupling of Nd and Hf isotopes along the Ganges floodplain is explained by
611 a change of river hydrodynamics, from a relatively turbulent regime that limited
612 mineralogical sorting within the water column at the mountain front, to a calmer regime
613 that allowed better mineral segregation in the floodplain and in the delta. Our
614 interpretation is further supported by the trace-element data shown in Figure 3. In
615 contrast to sediments from the Narayani, Karnali and Kosi Rivers (Figure 3f-g-h),
616 bedloads and bank sediments from the Bangladesh delta show significantly higher REE,
617 Th, U, Zr and Hf concentrations than suspended loads (Figure 3e). As shown in section
618 5.2.1, such differences reflect a higher degree of mineral sorting, in agreement with the
619 large differences of ε_{Hf} values observed between bedloads and suspended loads in the
620 Bangladesh delta (Figure 9).

621 The impact of mineralogical sorting processes on the overall chemistry of bed
622 and suspended loads from other large fluvial systems was highlighted in previous
623 studies (e.g. Gaillardet et al., 1995; Dupré et al., 1996; Bouchez et al., 2011). For example,
624 Bouchez et al. (2011) showed that mineral sorting of sediments explains a large part of

the chemical variability of bedloads and suspended loads in the Amazon River, another large fluvial system in terms of sediment discharge into the world ocean (Milliman and Meade, 1983; Milliman, 2001). Based on this observation, we suggest that Nd-Hf isotopic decoupling of river sediments is not restricted to the Ganges but may occur in all detrital sediments that are delivered into the ocean at the mouths of large rivers. Our results may thus explain why detrital oceanic clays are displaced towards elevated ε_{Hf} relative their ε_{Nd} values.

5.4. Impact of continental fractionation on oceanic sediments

Detrital sediments are transported from continent to ocean by rivers, glaciers or winds. The present flux of riverine sediment from continent to ocean is estimated at about 20 x 10^{12} kg.y^{-1} (Milliman and Meade, 1983; Hay, 1998 and references therein) while the estimated present flux for glacial detritus ranges between 0.9 and 50 x 10^{12} kg.y^{-1} and between 0.5 and 0.9 x 10^{12} kg.y^{-1} for dust (Hay, 1998 and references therein).

Here we evaluate whether the mineral sorting processes responsible for the Nd-Hf isotopic decoupling in river sediments can explain the range of isotopic compositions reported for worldwide terrigenous oceanic sediments (i.e. sand and clay). We do not discuss the composition of biogenic sediments and Fe-Mn crusts and nodules because their composition reflects that of dissolved Nd and Hf in seawater (e.g. Godfrey et al., 2009; Rickli et al., 2009; Zimmerman et al., 2009; Stichel et al., 2012) and our study focuses on particle loads. We use the vertical deviation from the Terrestrial Array ($\Delta\varepsilon$Hf) (cf. Figure 8) to compare river and oceanic sediments. Part of the amplitude of $\Delta\varepsilon$Hf values of worldwide sediments depends on the average age of the continental sources, which can be evaluated using their ε_{Nd} values. Sediments eroded from old evolved crust have very low ε_{Nd} values, and contain zircons with very low ε_{Hf} and phyllosilicates with

650 elevated ε_{Hf}. The range of ΔεHf should thus be very large. In contrast, erosion products of
651 younger crust have higher ε_{Nd} values, and the ε_{Hf} values of both zircons and
652 phyllosilicates are less extreme. The correction made to normalize the ε_{Hf} values of
653 sediments for the age effect is explained in the sketch shown in the inset of Figure 10.
654 We projected all initial Nd-Hf isotopic compositions of sediments to an arbitrary
655 intermediate ε_{Nd} value of -15 using straight lines that converge at an average depleted
656 mantle value of ε_{Nd} = +8.9 and ε_{Hf} = +14.8 (see caption of Figure 10). We then calculated
657 the vertical deviation ($\Delta\varepsilon_{Hf}$) from the Terrestrial Array of all projected ε_{Hf} values to
658 obtain a parameter that is not influenced by the age effect. Such a projection allows us to
659 compare sediments from everywhere in the world. It can be noted that $\Delta\varepsilon_{Hf}$ projected at
660 ε_{Nd}=-15 is a robust parameter since the trend that we observe for river and oceanic
661 sediments does not significantly change when we choose other reasonable values for the
662 depleted mantle or for the ε_{Nd} value at which the projection is done.

663 The range of normalized $\Delta\varepsilon_{Hf}$ is plotted in Figure 10 as a function of Al_2O_3/Zr
664 ratios for river and oceanic sediments. Like Vervoort et al. (2011), we selected Al_2O_3/Zr
665 instead of Al_2O_3/SiO_2 as proxy to the relative proportions of zircons vs. phyllosilicates
666 because the presence of biogenic silica in oceanic sediments affects Al_2O_3/SiO_2. Figure
667 10 shows that river and terrigenous oceanic sediments plot on the same trend in the
668 $\Delta\varepsilon_{Hf}$ vs Al_2O_3/Zr diagram. This suggests strongly that the decoupling of Nd and Hf
669 isotopic compositions in river and oceanic sediments results from the same process i.e.
670 mineral sorting, as suggested by Patchett et al. (1984). Oceanic sands and silts have $\Delta\varepsilon_{Hf}$
671 values similar to those of the Himalayan river sediments analyzed in this study, while
672 oceanic clays have generally higher $\Delta\varepsilon_{Hf}$ than the Himalayan suspended loads. This
673 shows that the decoupling observed in river sediments is amplified in the oceanic
674 environment. This arises because more than 90% of suspended matter transported by

675 rivers and nearly all bedloads are deposited in deltas and estuaries and never reach the
676 ocean (Lisitzin, 1996). Zircon is quantitively removed from suspended matter during
677 transport from river mouth to open ocean (Stummeyer et al., 2002). Sorting processes at
678 the river/ocean interface thus amplify chemical fractionation observed in rivers: they
679 sequester zircon-rich sediments with unradiogenic Hf signature and deliver sediments
680 with radiogenic Hf to the ocean. Almost half of the Nd-Hf isotopic decoupling occurs in
681 rivers on continents (see Figure 10) but Hf-Nd fractionation most probably continues as
682 fine particles travel far from continents while coarser fractions sediment close to source
683 areas.

684 Our study on river sediments shows that mineral sorting controls Nd-Hf
685 decoupling in both continental and oceanic environments. The displacement of Nd-Hf
686 isotopic compositions of terrigenous oceanic clays above the Terrestrial Array in Nd-Hf
687 isotopic space is similar to that observed on continents during transport from sediment
688 sources to the open ocean. If the Nd-Hf isotopic compositions of oceanic sediments differ
689 from those of continental crust, their recycling in subduction zones should influence the
690 long-term evolution of the Earth's mantle. Indeed, Chauvel et al. (2008) showed that an
691 input of oceanic sediment is needed to explain both the Mantle Array and the mantle
692 sources of oceanic island basalts (OIB) and mid-ocean ridge basalts (MORB). Here, we go
693 one step further and propose that reinjection of oceanic sediments into the mantle has
694 shifted the Terrestrial Array towards higher ε_{Hf} at high ε_{Nd} values over Earth history and
695 has resulted in a systematic change of the slope of the array. To demonstrate this, we
696 estimate what would be the present-day Nd-Hf isotopic composition of the depleted
697 mantle if sediments and oceanic crust had not been recycled into the mantle through
698 Earth history, i.e., we calculate the composition of the depleted mantle without recycled
699 material. To do this, we need to know the present-day isotopic compositions of oceanic

700 sediments and oceanic crust that had formed at different times in the past (green and
701 pink lines in Figure 11, see Figure caption and Chauvel et al., 2008 for further details
702 about the calculations). As a rough guide, we also show the evolution of continental
703 crust and OIB through time (blue and orange lines in Figure 11). All parameters used to
704 calculate the evolution of these reservoirs are provided in Supplementary Table D. We
705 calculate an average composition for recycled oceanic crust and overlying sediments
706 (grey star in Figure 11) assuming a mixture of 10-20% oceanic sediment and 80-90%
707 oceanic crust (same procedure as in Chauvel et al., 2008) and an average age of 1.8 Ga
708 (i.e. the average age of the continental crust). Assuming that the present-day depleted
709 mantle – the source of MORB shown with a pink star in Figure 11 – consists in a mixture
710 of 90-95% depleted mantle without recycled material and 5-10% recycled material
711 (Chauvel et al., 2008; Sobolev et al., 2007), we can estimate the present-day isotopic
712 composition of the depleted mantle without recycled material. This is shown by the grey
713 field in Figure 11. The exact location of this field depends on the parameters used for
714 mixing calculations and in particular the Nd and Hf concentrations of the depleted
715 mantle. As we choose relatively high Nd and Hf concentrations (see Supplementary
716 Table D), our grey field defines the lowest possible range of ε_{Hf} and ε_{Nd} values. If we
717 choose lower Nd and Hf concentrations, for example those of Salters and Stracke (2004),
718 the depleted mantle without recycled material remains below the mantle array and has
719 a much more radiogenic isotopic composition, as shown by the dashed grey field in
720 Figure 11. The principal result is that the composition of the depleted mantle without
721 recycled material differs significantly from that of MORB and always lies at elevated ε_{Nd}
722 values below the Terrestrial array. This suggests that mantle-derived materials formed
723 in the earliest part of history probably had lower ε_{Hf} at any given ε_{Nd} than recently
724 formed material. Evaluating the impact of such a temporal change using the composition

of old continental crust and mantle is difficult because data on old and well-constrained materials are not numerous. Additional Nd and Hf isotopic data on carefully selected rocks with ages covering the Earth history could provide further constraints.

The Terrestrial Array that describes the overall relationship between Nd and Hf isotopes is based on all available terrestrial data (Vervoort et al., 1999; Vervoort et al., 2011). Not only does it represent a mixture of materials formed at different times from the mantle but it also is strongly influenced by the large number of analyses obtained on recent basalts. We thus suggest that the slightly positive ε_{Hf} intercept and, more significantly, the large envelope of data surrounding the best-fit line through the Terrestrial Array could be due to the temporal increase of incongruence of the two isotopic systems.

6. Summary and Conclusions

This paper describes the first comprehensive study of Nd and Hf isotopic compositions in bedloads, suspended loads and bank sediments sampled along one of the largest rivers, the Ganges. Because source heterogeneity does not significantly affect the isotopic composition of the studied sediments, we could demonstrate that mineral sorting processes control the chemistry of Ganges river sediments and account for their entire Hf isotopic variability (>10 ε_{Hf}). Bedload and bank sediments always have lower ε_{Hf} than suspended loads sampled at the same location. As suggested by Patchett et al. (1984) for detrital oceanic sediments, coarse-grained sediments fall next to the Terrestrial Array in Hf-Nd isotopic space while fine-grained sediments display increasing decoupling of the two isotopic systems as sediment grain size decreases. We attribute these features to hydraulic sorting of minerals during transport on the floodplain, with the selective deposition of zircons that host significant amounts of

unradiogenic Hf. Zircons dominate the Hf isotopic budget of coarse sediments while their contribution to the Hf isotopic budget of finer sediments is balanced by minerals with more radiogenic Hf such as phyllosilicates.

We show that the Nd-Hf isotopic decoupling increases from mountain source to the estuary where it reaches its maximum. Decoupling of Nd and Hf isotopes in river sediments and oceanic clays is caused by the same processes, i.e., mineral sorting during transport. We speculate that transport of fine particles over long distances in the open ocean amplifies the signal. Finally, the recycling of oceanic sediments with anomalous Nd-Hf isotopic compositions into the mantle, would have slowly shifted the overall isotopic composition of the Earth's mantle towards more radiogenic Hf values.

Acknowledgments:

We thank A. Galy, M. Lupker, V. Galy and M. Attal who collected most of the samples analyzed in this study, S. Bureau for her help in the clean lab, P. Telouk (ENS, Lyon) for assistance during MC-ICP-MS measurements at Lyon and N. Arndt (ISTerre, Grenoble) for discussions that improved the style and the content of the manuscript. We are also grateful to Julie Prytulak, two anonymous reviewers and the associate editor Steve Shirey for their very constructive comments on the manuscript. This study was supported by funding from CNRS and INSU programs.

References

Ahmad T., Harris N., Bickle M., Chapman H., Bunbury J. and Prince C. (2000) Isotopic constraints on the structural relationships between the lesser Himalayan series and the high Himalayan crystalline series, Garhwal Himalaya. *Geological Society of America Bulletin* **112**, 467–477.

775 Albarède F., Goldstein S. L. and Dautel D. (1997) The neodymium isotopic composition of
776 manganese nodules from the Southern and Indian oceans, the global oceanic
777 neodymium budget, and their bearing on deep ocean circulation. *Geochimica et*
778 *Cosmochimica Acta* **61**, 1277–1291.

779 Albarède F., Simonetti A., Vervoort J. D., Blichert-Toft J. and Abouchami W. (1998) A Hf-
780 Nd isotopic correlation in ferromanganese nodules. *Geophys. Res. Lett.* **25**, 3895–
781 3898.

782 Attal M. and Lavé J. (2006) Changes of bedload characteristics along the Marsyandi River
783 (central Nepal): Implications for understanding hillslope sediment supply, sediment
784 load evolution along fluvial networks, and denudation in active orogenic belts.
785 *Geological Society of America Special Paper* **398**, 143–171.

786 Bayon G., Burton K. W., Soulet G., Vigier N., Dennielou B., Etoubleau J., Ponzevera E.,
787 German C. R. and Nesbitt R. W. (2009) Hf and Nd isotopes in marine sediments:
788 Constraints on global silicate weathering. *Earth and Planetary Science Letters* **277**,
789 318–326.

790 Bayon G., Vigier N., Burton K. W., Jean Carignan A. B., Etoubleau J. and Chu N.-C. (2006)
791 The control of weathering processes on riverine and seawater hafnium isotope
792 ratios. *Geology* **34**, 433.

793 Bau M. and Koschinsky A. (2006) Hafnium and neodymium isotopes in seawater and in
794 ferromanganese crusts: The "element perspective." *Earth and Planetary Science*
795 *Letters* **241**, 952–961.

796 Ben Othman D., White W. M. and Patchett J. (1989) The geochemistry of marine

797 sediments, island arc magma genesis, and crust-mantle recycling. *Earth and*
798 *Planetary Science Letters* **94**, 1–21.

799 Bouchez J., Gaillardet J., France-Lanord C., Maurice L. and Dutra-Maia P. (2011) Grain
800 size control of river suspended sediment geochemistry: Clues from Amazon River
801 depth profiles. *Geochem. Geophys. Geosyst.* **12**, Q03008.

802 Bouvier A., Vervoort J. D. and Patchett P. J. (2008) The Lu–Hf and Sm–Nd isotopic
803 composition of CHUR: constraints from unequilibrated chondrites and implications
804 for the bulk composition of terrestrial planets. *Earth and Planetary Science Letters*
805 **273**, 48–57.

806 Carignan J., Hild P., Mevelle G., Morel J. and Yeghicheyan D. (2007) Routine Analyses of
807 Trace Elements in Geological Samples using Flow Injection and Low Pressure On-
808 Line Liquid Chromatography Coupled to ICP-MS: A Study of Geochemical Reference
809 Materials BR, DR-N, UB-N, AN-G and GH. *Geostandards and Geoanalytical Research*
810 **25**, 187–198.

811 Carpentier M., Chauvel C. and Mattielli N. (2008) Pb–Nd isotopic constraints on
812 sedimentary input into the Lesser Antilles arc system. *Earth and Planetary Science*
813 *Letters* **272**, 199–211.

814 Carpentier M., Chauvel C., Maury R. C. and Mattielli N. (2009) The "zircon effect" as
815 recorded by the chemical and Hf isotopic compositions of Lesser Antilles forearc
816 sediments. *Earth and Planetary Science Letters* **287**, 86–99.

817 Chauvel C. and Blichert-Toft J. (2001) A hafnium isotope and trace element perspective
818 on melting of the depleted mantle. *Earth and Planetary Science Letters* **190**, 137–

151.

Chauvel C., Bureau S. and Poggi C. (2011) Comprehensive chemical and isotopic analyses of basalt and sediment reference materials. *Geostandards and Geoanalytical Research* **35**, 125–143.

Chauvel C., Lewin E., Carpentier M., Arndt N. T. and Marini J.-C. (2008) Role of recycled oceanic basalt and sediment in generating the Hf–Nd mantle array. *Nature Geosciences* **1**, 64–67.

Chauvel C., Marini J.-C., Plank T. and Ludden J. N. (2009) Hf-Nd input flux in the Izu-Mariana subduction zone and recycling of subducted material in the mantle. *Geochem. Geophys. Geosyst.* **10**, Q01001.

Chen T.-Y., Ling H.-F., Frank M., Zhao K.-D. and Jiang S.-Y. (2011) Zircon effect alone insufficient to generate seawater Nd-Hf isotope relationships. *Geochem. Geophys. Geosyst.* **12**, Q05003, doi:10.1029/2010GC003363.

Condie K. C. (1991) Another look at rare earth elements in shales. *Geochimica et Cosmochimica Acta* **55**, 2527–2531.

Curray J. R. (1994) Sediment volume and mass beneath the Bay of Bengal. *Earth and Planetary Science Letters* **125**, 371–383.

Curray J. R., Emmel F. J. and Moore D. G. (2003) The Bengal Fan: morphology, geometry, stratigraphy, history and processes. *Marine and Petroleum Geology* **19**, 1191–1223.

David K., Frank M., O'Nions R., Belshaw N. and Arden J. (2001) The Hf isotope composition of global seawater and the evolution of Hf isotopes in the deep Pacific

840 Ocean from Fe-Mn crusts. *Chemical Geology* **178**, 23–42.

841 Dupré B., Gaillardet J., Rousseau D. and Allègre C. J. (1996) Major and trace elements of
842 river-borne material: The Congo Basin. *Geochimica et Cosmochimica Acta* **60**, 1301–
843 1321.

844 France-Lanord C., Derry L. and Michard A. (1993) Evolution of the Himalaya since
845 Miocene time: isotopic and sedimentological evidence from the Bengal Fan.
846 *Geological Sociiety of London* **74**, 603–621.

847 Gaillardet J., Dupré B. and Allègre C. J. (1995) A global geochemical mass budget applied
848 to the Congo Basin rivers: Erosion rates and continental crust composition.
849 *Geochimica et Cosmochimica Acta* **59**, 3469–3485.

850 Gale A., Dalton C. A., Langmuir C. H., Su Y. and Schilling J.-G. (2013) The mean
851 composition of ocean ridge basalts. *Geochem. Geophys. Geosyst.* **14**, 489–518, doi:
852 10.1029/2012GC004334.

853 Galy A. and France-Lanord C. (2001) Higher erosion rates in the Himalaya: Geochemical
854 constraints on riverine fluxes. *Geology* **29**, 23–26.

855 Galy A. and France-Lanord C. (1999) Weathering processes in the Ganges–Brahmaputra
856 basin and the riverine alkalinity budget. *Chemical Geology*, 31–60.

857 Galy V., France-Lanord C. and Lartiges B. (2008) Loading and fate of particulate organic
858 carbon from the Himalaya to the Ganga–Brahmaputra delta. *Geochimica et*
859 *Cosmochimica Acta* **72**, 1767–1787.

860 Galy V., France-Lanord C., Beyssac O., Faure P., Kudrass H. and Palhol F. (2007) Efficient

organic carbon burial in the Bengal fan sustained by the Himalayan erosional system. *Nature* **450**, 407–410.

Garçon M., Chauvel C. and Bureau S. (2011) Beach placer, a proxy for the average Nd and Hf isotopic composition of a continental area. *Chemical Geology*, 1–11.

Garzanti E., Andò S., France-Lanord C., Censi P., Pietro Vignola, Galy V. and Lupker M. (2011) Mineralogical and chemical variability of fluvial sediments 2. Suspended-load silt (Ganga–Brahmaputra, Bangladesh). *Earth and Planetary Science Letters* **302**, 107–120.

Garzanti E., Andò S., France-Lanord C., Vezzoli G., Censi P., Galy V. and Najman Y. (2010) Mineralogical and chemical variability of fluvial sediments 1. Bedload sand (Ganga – Brahmaputra, Bangladesh). *Earth and Planetary Science Letters* **299**, 368–381.

Garzanti E., Vezzoli G., Andò S., lavé J., Attal M., France-Lanord C. and Decelles P. G. (2007) Quantifying sand provenance and erosion (Marsyandi River, Nepal Himalaya). *Earth and Planetary Science Letters* **258**, 500–515.

Godfrey L. V., Zimmermann B., Lee D.-C., King R. L., Vervoort J. D., Sherrell R. M. and Halliday A. N. (2009) Hafnium and neodymium isotope variations in NE Atlantic seawater. *Geochem. Geophys. Geosyst.* **10**, Q08015, doi:10.1029/2009GC002508.

Godfrey L., Lee D.-C., Sangrey W., Halliday A., Salters V., Hein J. and White W. (1997) The Hf isotopic composition of ferromanganese nodules and crusts and hydrothermal manganese deposits: Implications for seawater Hf. *Earth and Planetary Science Letters* **151**, 91–105.

Goldstein S. and Jacobsen S. B. (1988) Nd and Sr isotopic systematics of river water

suspended material: implications for crustal evolution. *Earth and Planetary Science Letters* **87**, 249–265.

Govindaraju K. and Mevelle G. (1987) Fully automated dissolution and separation methods for inductively coupled plasma atomic emission spectrometry rock analysis. Application to the determination of rare earth elements. Plenary lecture. *J. Anal. At. Spectrom.* **2**, 615–621.

Götze J. and Lewis R. (1994) Distribution of REE and trace elements in size and mineral fractions of high-purity quartz sands. *Chemical Geology* **114**, 43–57.

Harrison T. M., Blichert-Toft J., Müller W., Albarède F., Holden P. and Mojzsis S. J. (2005) Heterogeneous Hadean Hafnium: Evidence of Continental Crust at 4.4 to 4.5 Ga. *Science* **310**, 1947–1950.

Hay W. W. (1998) Detrital sediment fluxes from continents to oceans. *Chemical Geology* **145**, 287–323.

Islam M. R., Begum S. F., Yamaguchi Y. and Ogawa K. (1999) The Ganges and Brahmaputra rivers in Bangladesh: basin denudation and sedimentation. *Hydrol. Process.* **13**, 2907–2923.

Kemp A. I. S., Hawkesworth C. J., Foster G. L., Paterson B. A., Woodhead J. D., Hergt J. M., Gray C. M. and Whitehouse M. J. (2007) Magmatic and Crustal Differentiation History of Granitic Rocks from Hf-O Isotopes in Zircon. *Science* **315**, 980–983.

Kinny P. D. and Maas R. (2003) Lu–Hf and Sm–Nd isotope systems in zircon. *Reviews in mineralogy and geochemistry* **53**, 327–341.

Le Fort P. (1975) Himalayas: the collided range. Present knowledge of the continental arc. *American Journal of Science* **275A**, 1–44.

Lisitzin A. P. (1996) *Oceanic Sedimentation: Lithology and Geochemistry*, American Geophysical Union, Washington, D. C.

Lupker M., France-Lanord C., Galy V., lavé J., Gaillardet J., Gajurel A. P., Guilmette C., Rahman M., Singh S. K. and Sinha R. (2012) Predominant floodplain over mountain weathering of Himalayan sediments (Ganga basin). *Geochimica et Cosmochimica Acta* **84**, 410-432.

Lupker M., France-Lanord C., lavé J., Bouchez J., Galy V., Métivier F., Gaillardet J., Lartiges B. and Mugnier J.-L. (2011) A Rouse-based method to integrate the chemical composition of river sediments: Application to the Ganga basin. *J. Geophys. Res.* **116**, F04012.

McLennan S. M., Taylor S. R., McCulloch M. T. and Maynard J. B. (1990) Geochemical and Nd-Sr isotopic composition of deep-sea turbidites: Crustal evolution and plate tectonic associations. *Geochimica et Cosmochimica Acta* **54**, 2015–2050.

Milliman J. D. (2001) River inputs, in Encyclopedia of Ocean Sciences, edited by J. H. Steele, K. K. Turekian, and S. A. Thorpe, pp. 2419–2427, Elsevier, New York.

Milliman J. and Meade R. H. (1983) World-wide delivery of river sediment to the oceans. *The Journal of Geology* **91**, 1–21.

Parrish R. R. and Hodges V. (1996) Isotopic constraints on the age and provenance of the Lesser and Greater Himalayan sequences, Nepalese Himalaya. *Geological Society of America Bulletin* **108**, 904–911.

926 Patchett P. J., White W. M., Feldmann H., Kielinczuk S. and Hofmann A. W. (1984)
927 Hafnium/rare earth element fractionation in the sedimentary system and crustal
928 recycling into the Earth's mantle. *Earth and Planetary Science Letters* **69**, 365–378.

929 Pearce J., Kempton P., Nowell G. and Noble S. (1999) Hf-Nd element and isotope
930 perspective on the nature and provenance of mantle and subduction components in
931 Western Pacific arc-basin systems. *Journal of Petrology* **40**, 1579–1611.

932 Pettke T., Lee D.-C., Halliday A. N. and Rea D. K. (2002) Radiogenic Hf isotopic
933 compositions of continental eolian dust from Asia, its variability and its implications
934 for seawater Hf. *Earth and Planetary Science Letters* **202**, 453–464.

935 Pierson-Wickmann A.-C., Reisberg L. and France-Lanord C. (2000) The Os isotopic
936 composition of Himalayan river bedloads and bedrocks: importance of black shales.
937 *Earth and Planetary Science Letters* **176**, 203–218.

938 Plank T., Kelley K. A., Murray R. W. and Stern L. Q. (2007) Chemical composition of
939 sediments subducting at the Izu-Bonin trench. *Geochem. Geophys. Geosyst.* **8**.

940 Prytulak J., Vervoort J. D., Plank T. and Yu C. (2006) Astoria Fan sediments, DSDP site
941 174, Cascadia Basin: Hf–Nd–Pb constraints on provenance and outburst flooding.
942 *Chemical Geology* **233**, 276–292.

943 Richards A., Argles T., Harris N., Parrish R., Ahmad T., Darbyshire F. and Draganits E.
944 (2005) Himalayan architecture constrained by isotopic tracers from clastic
945 sediments. *Earth and Planetary Science Letters* **236**, 773–796.

946 Rickli J., Frank M. and Halliday A. N. (2009) The hafnium–neodymium isotopic
947 composition of Atlantic seawater. *Earth and Planetary Science Letters* **280**, 118–127.

948 Rickli J., Frank M., Baker A. R., Aciego S., de Souza G., Georg R. B. and Halliday A. N.
949 (2010) Hafnium and neodymium isotopes in surface waters of the eastern Atlantic
950 Ocean: Implications for sources and inputs of trace metals to the ocean. *Geochimica*
951 *et Cosmochimica Acta* **74**, 540–557.

952 Rickli J., Frank M., Stichel T., Georg R. B., Vance D. and Halliday A. N. (2013) Controls on
953 the incongruent release of hafnium during weathering of metamorphic and
954 sedimentary catchments. *Geochimica et Cosmochimica Acta* **101**, 263–284.

955 Robinson D. M., Decelles P. G., Patchett P. J. and Garzione C. N. (2001) The kinematic
956 evolution of the Nepalese Himalaya interpreted from Nd isotopes. *Earth and*
957 *Planetary Science Letters* **192**, 507–521.

958 Rudnick R. L. and Gao S. (2003) The Composition of the Crust. In *The Crust Vol.3 Treatise*
959 *on Geochemistry* (ed. R. L. Rudnick). pp. 1–64.

960 Salters V. J. and Stracke A. (2004) Composition of the depleted mantle. *Geochem.*
961 *Geophys. Geosyst. 5,* Q05004, doi:10.1029/2003GC000597*.*

962 Singh M., Singh I. B. and Müller G. (2007) Sediment characteristics and transportation
963 dynamics of the Ganga River. *Geomorphology* **86**, 144–175.

964 Singh P. (2010) Geochemistry and provenance of stream sediments of the Ganga River
965 and its major tributaries in the Himalayan region, India. *Chemical Geology* **269**, 220–
966 236.

967 Singh P. (2009) Major, trace and REE geochemistry of the Ganga River sediments:
968 Influence of provenance and sedimentary processes. *Chemical Geology* **266**, 242–
969 255.

970 Singh S. K. and France-Lanord C. (2002) Tracing the distribution of erosion in the

971 Brahmaputra watershed from isotopic compositions of stream sediments. *Earth and*
972 *Planetary Science Letters* **202**, 645–662.

973 Singh S. K., Rai S. K. and Krishnaswami S. (2008) Sr and Nd isotopes in river sediments
974 from the Ganga Basin: Sediment provenance and spatial variability in physical
975 erosion. *J. Geophys. Res.* **113**, F03006.

976 Sobolev A. V., Hofmann A. W., Kuzmin D. V., Yaxley G. M., Arndt N. T., Chung S.-L.,
977 Danyushevsky L. V., Elliott T., Frey F. A. and Garcia M. O. (2007) The amount of
978 recycled crust in sources of mantle-derived melts. *Science* **316**, 412–417.

979 Stichel T., Frank M., Rickli J. and Haley B. A. (2012) The hafnium and neodymium isotope
980 composition of seawater in the Atlantic sector of the Southern Ocean. *Earth and*
981 *Planetary Science Letters* **317-318**, 282–294.

982 Stummeyer J., Marchig V. and Knabe W. (2002) The composition of suspended matter
983 from Ganges–Brahmaputra sediment dispersal system during low sediment
984 transport season. *Chemical Geology* **185**, 125–147.

985 Taylor S. R. and McLennan S. M. (1995) The Geochemical evolution of the Continental
986 Crust. *Reviews of Geophysics* **33**, 241–265.

987 Totten M. (2007) Developments in Sedimentology - Chapter 12 Heavy Minerals in
988 Shales. *Developments in Sedimentology*.

989 Tripathi J. K., Ghazanfari P., Rajamani V. and Tandon S. (2007) Geochemistry of
990 sediments of the Ganges alluvial plains: Evidence of large-scale sediment recycling.
991 *Quaternary International* **159**, 119–130.

992 van de Flierdt T., Frank M., Lee D.-C., Halliday A. N., Reynolds B. C. and Hein J. R. (2004)

New constraints on the sources and behavior of neodymium and hafnium in seawater from Pacific Ocean ferromanganese crusts. *Geochimica et Cosmochimica Acta* **68**, 3827–3843.

van de Flierdt T., Goldstein S. L., Hemming S. R., Roy M., Frank M. and Halliday A. N. (2007) Global neodymium–hafnium isotope systematics—revisited. *Earth and Planetary Science Letters* **259**, 432–441.

van De Flierdt T., Hemming S. R., Goldstein S. L. and Abouchami W. (2006) Radiogenic isotope fingerprint of Wilkes Land–Adélie Coast Bottom Water in the circum-Antarctic Ocean. *Geophys. Res. Lett.* **33**, L12606.

Vervoort J. D., Patchett P. D., Blichert-Toft J. and Albarède F. (1999) Relationships between Lu–Hf and Sm–Nd isotopic systems in the global sedimentary system. *Earth and Planetary Science Letters* **168**, 79–99.

Vervoort J., Plank T. and Prytulak J. (2011) The Hf-Nd isotopic composition of marine sediments. *Geochimica et Cosmochimica Acta* **75**, 5903-5926.

Viers J., Roddaz M., Filizola N., Guyot J.-L., Sondag F., Brunet P., Zouiten C., Boucayrand C., Martin F. and Boaventura G. R. (2008) Seasonal and provenance controls on Nd–Sr isotopic compositions of Amazon rivers suspended sediments and implications for Nd and Sr fluxes exported to the Atlantic Ocean. *Earth and Planetary Science Letters* **274**, 511–523.

Vlastélic I. (2005) Miocene climate change recorded in the chemical and isotopic (Pb, Nd, Hf) signature of Southern Ocean sediments. *Geochem. Geophys. Geosyst.* **6**, Q03003.

White W. M., Patchett J. and BenOthman D. (1986) Hf isotope ratios of marine sediments

and Mn nodules: evidence for a mantle source of Hf in seawater. *Earth and Planetary Science Letters* **79**, 46–54.

Woodhead J., Hergt J., Davidson J. and Eggins S. (2001) Hafnium isotope evidence for "conservative"element mobility during subduction zone processes. *Earth and Planetary Science Letters* **192**, 331–346.

Zimmermann B., Porcelli D., Frank M., Rickli J., Lee D.-C. and Halliday A. N. (2009) The hafnium isotope composition of Pacific Ocean water. *Geochimica et Cosmochimica Acta* **73**, 91–101.

Table Captions

Table 1: Nf and Hf isotopes in river sediments

Footnotes: Re-run samples correspond to run duplicates and Dup samples stand for complete analytical duplicates. Uncertainties (± 2σ) indicated in the Table are in-run errors. ε_{Nd} and ε_{Hf} values were calculated using the CHUR composition published by (Bouvier et al., 2008).

Figure Captions

Figure 1: Map of the Ganges fluvial system showing the main sampling sites for the river sediments analyzed in this study.

Footnotes: Blue stars indicate the locations of samples from the Ganges River, red stars those from the Karnali River, purple stars those from the Narrayani river, yellow stars those from the Kosi River. White, light and dark grey stars indicate the locations of the samples from Nepalese rivers draining the Lesser Himalaya units, the High Himalayan

1038 Crystalline units and the Tethyan Sedimentary Series, respectively. The precise locations
1039 can be found in Pierson-Wickmann et al. (2000) and Garzanti et al. (2007) while their
1040 GPS coordinates are provided in Supplementary Table B. Detailed locations of the 10
1041 samples recovered in the Marsyandi River (pink star) can be found in Garzanti et al.
1042 (2007) and GPS coordinates are provided in Supplementary Table B.
1043
1044 **Figure 2: a)** Variability of SiO_2 and Al_2O_3 contents in river sediments. **b)** Histogram
1045 showing the frequency of Al_2O_3/SiO_2 ratios for the studied bedloads, banks and
1046 suspended loads.
1047 *Footnotes*: Red and green stars correspond to the average composition of the Ganges
1048 bedload and surface suspended load in Bangladesh, as published by Lupker et al. (2011).
1049 The composition of the average Upper Continental Crust (Rudnick and Gao, 2003) is
1050 shown as indication.
1051
1052 **Figure 3:** Trace element patterns normalized to the average composition of the upper
1053 continental crust (UCC) of Rudnick and Gao (2003) for sediments sampled in rivers
1054 draining single geological units (a-b-c) as well as in the Marsyandi (d), the Ganges (e),
1055 the Narayani (f), the Karnali (g) and the Kosi rivers (h).
1056
1057 **Figure 4:** ε_{Hf} versus ε_{Nd} diagram showing river sediments sampled in the Himalayan
1058 Range i.e. in the Marsyandi River and in small Nepalese rivers draining only the Tethyan
1059 Sedimentary Series, the High Himalayan Crystalline and the Lesser Himalaya.
1060 *Footnotes:* Nd-Hf isotopic compositions of worldwide oceanic sediments are also shown.
1061 Data for Fe-Mn crusts and nodules are from Albarède et al. (1997); Godfrey et al. (1997);
1062 Albarède et al. (1998); David et al. (2001); van De Flierdt et al. (2006); oceanic clays and

biogenic muds are from White et al. (1986); Ben Othman et al. (1989); McLennan et al. (1990); Pearce et al. (1999); Vervoort et al. (1999); Woodhead et al. (2001); Vlastélic (2005); Prytulak et al. (2006); Carpentier et al. (2008); Bayon et al. (2009); Carpentier et al. (2009); Chauvel et al. (2009); Vervoort et al. (2011) and oceanic silts and sands are from McLennan et al. (1990); Vervoort et al. (1999); Prytulak et al. (2006); Carpentier et al. (2008); Bayon et al. (2009); Carpentier et al. (2009); Vervoort et al. (2011). The present-day Terrestrial Array is that of Vervoort et al. (2011). The histogram along the ε_{Nd} axis shows ε_{Nd} values reported for Himalayan bedrocks from the three main geological units (Parrish and Hodges, 1996; Ahmad et al., 2000; Robinson et al., 2001; Richards et al., 2005). All ε_{Nd} and ε_{Hf} values were recalculated using the CHUR composition published by Bouvier et al. (2008).

Figure 5: ε_{Hf} versus ε_{Nd} diagram showing data obtained on sediments sampled in the floodplain i.e. in the Ganges and its main tributaries.

Footnotes: Same sources of data as in Figure 4. ε_{Nd} and ε_{Hf} values calculated using the CHUR composition published by Bouvier et al. (2008).

Figure 6: Downstream evolution of ε_{Nd} and ε_{Hf} in sediments along the Marsyandi River located in the Himalayan Range.

Footnotes: The river profile and the main geological units on which the river flows are shown together with the location of two towns, Tal and Besi Shahar.

Figure 7: Variations of ε_{Hf} and ε_{Nd} as a function of Al_2O_3/SiO_2 ratio used as a grain-size proxy for the Ganges, the Narayani, the Karnali and the Kosi river sediments.

Footnotes: The color lines link bedloads and banks to their corresponding suspended loads sampled at the same location at different depths in the water column.

Figure 8: $\Delta\varepsilon_{Hf}$ vs. Al_2O_3/SiO_2 ratio used as grain-size proxy for the Ganges, the Narayani, the Karnali and the Kosi river sediments.

Footnotes: The sketch at the bottom right corner shows how vertical deviations ($\Delta\varepsilon_{Hf}$) from the present-day Terrestrial Array of Vervoort et al. (2011) are calculated.

Figure 9: Downstream changes of ε_{Nd} and ε_{Hf} in sediments from the Ganges and its major tributaries in the floodplain, from the Himalayan Mountain front to the Bengal delta.

Footnotes: Same symbols and colors as in previous figures. Color lines link bedloads and banks to their corresponding suspended loads sampled at the same location at different depths in the water column. The topography of the river profile is shown in brown.

Figure 10: $\Delta\varepsilon_{Hf}$ projected at ε_{Nd}=-15 plotted as a function of Al_2O_3/Zr ratios for river sediments analyzed in this study and worldwide oceanic terrigenous sediments (oceanic sands, silts and clays).

Footnotes: The sketch shown in the inset explains how all measured and published ε_{Hf} are projected to ε_{Nd}=-15 to calculate the vertical deviation from the present-day Terrestrial Array of Vervoort et al. (2011): $\Delta\varepsilon_{Hf}$ that is plotted in the main panel. The ε_{Nd} value of the depleted mantle pole was compiled using data from the PETDB database and its ε_{Hf} was calculated by projecting this ε_{Nd} value on the Terrestrial Array of Vervoort et al. (2011). In the main panel, colors and symbols for river sediments analyzed in this study are the same as in previous figures. Data for oceanic sands, silts

and clays correspond to terrigenous sediments poor in volcanic ashes and are from Plank et al. (2007); Carpentier et al. (2008); Carpentier et al. (2009); Chauvel et al. (2009); Vervoort et al. (2011). ε_{Hf} and ε_{Nd} of terrigenous sediments have been corrected for subsequent decay after their deposition age.

Figure 11: Present-day Nd-Hf isotopic compositions of the different Earth reservoirs and our estimated values for the depleted mantle without recycled material.

Footnotes: The present-day Nd-Hf isotopic compositions of oceanic sediments are from Chauvel et al. (2008). Present-day Nd isotopic compositions of MORB and OIB are from Gale et al. (2013) and PetDB database, respectively. Hf isotopic compositions of MORB and OIB were calculated from their Nd isotopic composition to lie on the present-day Terrestrial Array of Vervoort et al. (2011). Colored lines show the present-day isotopic compositions of oceanic sediments, continental crust, OIB and MORB that had formed at different times in the past. To model these evolutions, we assumed a linear relationship between the present-day isotopic compositions of the reservoirs and the Nd-Hf isotopic ratios of the Earth at 4.55 Ga. Oceanic sediments, continental crust, OIB and MORB are then modeled to evolve through time following their own Sm/Nd and Lu/Hf ratios (see Supplementary Table D). The grey star shows the average Nd-Hf isotopic composition of the material being recycled in the mantle. It is calculated using a binary mixing between 10-20% of 1.8 Ga oceanic sediment and 80-90% of 1.8 Ga oceanic crust (black mixing line with ticks indicating the proportion of sediment in the mixture). The field of present-day values for the depleted mantle without recycled material (grey field) was calculated assuming that the present-day depleted mantle (average MORB) results of a mixture of 5-10% recycled material and 90-95% depleted mantle without recycled material (grey mixing line). The dashed grey field shows the composition of the same

reservoir if the MORB source has very low Nd and Hf concentrations (i.e. 0.713 ppm for Nd and 0.199 ppm for Hf; Salters and Stracke, 2004).

Table 1

Table 1: Hf and Nd isotopes in sediments

From rivers draining monolithologic basins in the Himalayan range

Sample Name	Locality	River	Type of sediment	$^{176}Hf/^{177}Hf$	± 2σ	εHf	$^{143}Nd/^{144}Nd$	± 2σ	εNd
Lesser Himalaya units									
R 94-12	Sarmi, Nepal	Tributary of the Bheri River	Bedload	0.281956	11	-29.3	0.511422	11	-23.6
MO 102	Darondi/Marsel, Nepal	Marsel Khola	Bank	0.281798	5	-34.9	0.511436	9	-23.3
MO 112	Bhuri Gandaki/Isul, Nepal	Isul Khola	Bank	0.281646	5	-40.3	0.511380	6	-24.4
MO 112 re-run							0.511379	6	-24.4
PB 33	Nepal	Ghara khola	Suspended Load	0.281972	9	-28.8	0.511577	8	-20.5
PB 37	Nepal	Beg Khola	Bank	0.281659	13	-39.8	0.511488	5	-22.3
PB 37 re-run							0.511488	5	-22.3
MO 207	Waling, Nepal	Andi Khola	Bedload	0.281672	20	-39.4	0.511343	7	-25.1
MO 207 re-run				0.281663	7	-39.7			
High Himalayan Crystalline units									
MO 73	Nepal	Tributary of the Chepe khola	Bank	0.282243	12	-19.2	0.511724	10	-17.7
MO 50	Nepal	Chepe khola	Bank	0.282427	13	-12.7	0.511968	5	-12.9
MO 59	Nepal	Chepe khola	Bank	0.282374	9	-14.5	0.511953	9	-13.2
MO 59 re-run				0.282348	5	-15.4			
KN 83	Ghyangphedi, Nepal	Tadi khola	Bedload	0.282156	10	-22.2	0.511811	6	-16.0
Tethyan Sedimentary Series									
MO 504	Tukche, Nepal	Yamkim khola	Suspended Load	0.282235	8	-19.5	0.511730	6	-17.6
NAG 22	Pedi, Nepal	Marsyandi (10 km away from the River Source)	Bedload	0.282175	9	-21.6	0.511779	5	-16.6
NAG 22 re-run					0		0.511778	6	-16.6
MAR-50	Temang, Nepal	Marsyandi (60 km away from the River Source)	Bedload	0.282138	8	-22.9	0.511760	6	-17.0
MAR-50 re-run				0.282146	11	-22.6	0.511756	5	-17.0
MAR-40	Sabche, Nepal	Sabche khola	Bedload	0.282114	8	-23.7	0.511693	6	-18.3
MAR-40 Dup							0.511695	8	-18.2

From the Marsyandi River in the Himalayan range

Sample Name	Locality	Distance from River Source (km)	Type of sediment	$^{176}Hf/^{177}Hf$	± 2σ	εHf	$^{143}Nd/^{144}Nd$	± 2σ	εNd
MAR-55	Tal, Nepal	72	Bedload	0.282202	9	-20.6	0.511798	7	-16.2
MAR-58	Chamje, Nepal	75	Bedload	0.282151	8	-22.4	0.511803	7	-16.1
MAR-70	Besi Sahar, Nepal	104	Bedload	0.282178	8	-21.5	0.511813	8	-15.9
MAR-31	Philesangu, Nepal	111	Bedload	0.282065	8	-25.5	0.511816	6	-15.9
MAR-29	Suribar, Nepal	119	Bedload	0.282207	8	-20.4	0.511715	6	-17.8
MAR-29 re-run							0.511724	8	-17.7
MAR-19	Turture, Nepal	133	Bedload	0.282222	6	-19.9	0.511841	6	-15.4
MAR-19 re-run				0.282218	9	-20.1			
MAR-12	Anpu, Nepal	161	Bedload	0.282126	9	-23.3	0.511803	5	-16.1
MAR-10	Lobrang, Nepal	166	Bedload	0.282189	6	-21.1	0.511724	7	-17.7
MAR-10 Dup	Lobrang, Nepal	166	Bedload	0.282219	11	-20.0	0.511709	7	-18.0

From the Ganga river and its major tributaries in the floodplain

Sample Name	Locality	Distance from River Source (km)	Type of sediment	$^{176}Hf/^{177}Hf$	± 2σ	εHf	$^{143}Nd/^{144}Nd$	± 2σ	εNd
Ganga River									
BR 931	Devrapayag, India	260	Suspended Load	0.282118	7	-23.6	0.511818	8	-15.8
BR 932	Devrapayag, India	260	Suspended Load	0.282070	6	-25.3	0.511724	5	-17.7
BR 922	Rishikesh, India	260	Suspended Load	0.282180	6	-21.4	0.511706	6	-18.0
BR 922 re-run							0.511715	7	-17.9

Sample Name	Locality	Distance from River Source (km)	Type of sediment	$^{176}Hf/^{177}Hf$	± 2σ	εHf	$^{143}Nd/^{144}Nd$	± 2σ	εNd
BR 924	Rishikesh, India	260	Bank	0.282053	7	-25.9	0.511737	7	-17.4
BR 943	Kanpur, India	800	Suspended Load	0.282217	8	-20.1	0.511829	6	-15.6
BR 946	Kanpur, India	800	Bedload	0.282055	5	-25.8	0.511780	8	-16.6
BR 946 Dup	Kanpur, India	800	Bedload	0.282004	8	-27.6	0.511728	5	-17.6
BGP 6	Rajshahi, India	2570	Bedload	0.282027	11	-26.8	0.511758	9	-17.0
BGP 6 re-run		2570					0.511752	6	-17.1
BGP 6 Dup	Rajshahi, India	2570	Bedload	0.282009	7	-27.5	0.511749	7	-17.2
BR 415	Harding bridge, Bangladesh	2640	Suspended Load	0.282241	9	-19.2	0.511752	6	-17.1
BR 414	Harding bridge, Bangladesh	2640	Suspended Load	0.282226	6	-19.8	0.511736	8	-17.4
BR 413	Harding bridge, Bangladesh	2640	Suspended Load	0.282205	6	-20.5	0.511748	6	-17.2
BR 413 re-run				0.282198	5	-20.8			
BR 412	Harding bridge, Bangladesh	2640	Suspended Load	0.282209	6	-20.4	0.511745	7	-17.3
BR 411	Harding bridge, Bangladesh	2640	Suspended Load	0.282133	7	-23.0	0.511755	6	-17.1
BR 411 Dup	Harding bridge, Bangladesh	2640	Suspended Load				0.511723	7	-17.7
BR 418	Harding bridge, Bangladesh	2640	Bedload	0.281992	11	-28.1	0.511719	5	-17.8
BR 8252	Harding bridge, Bangladesh	2640	Bedload				0.511788	11	-16.4
BR 8253	Harding bridge, Bangladesh	2640	Suspended Load	0.282268	7	-18.3	0.511767	8	-16.8
BR 717	Harding bridge, Bangladesh	2640	Bedload	0.281930	6	-30.2	0.511769	7	-16.8
BR 717 re-run				0.281944	8	-29.8			
Karnali River									
PB 79	Chisapani, Nepal	260	Suspended Load	0.282155	8	-22.3	0.511721	6	-17.7
PB 79 re-run							0.511717	6	-17.8
PB 80	Chisapani, Nepal	260	Bank	0.282033	8	-26.6	0.511775	8	-16.7
BR 8113	Revelganj, India	850	Suspended Load	0.282206	6	-20.5	0.511758	7	-17.0
BR 8113 re-run							0.511744	6	-17.3
BR 8113 Dup	Revelganj, India	850	Suspended Load	0.282192	6	-21.0			
BR 8115	Revelganj, India	850	Bedload	0.282027	8	-26.8	0.511684	6	-18.5
BR 8115 Dup	Revelganj, India	850	Bedload				0.511714	9	-17.9
BR 8115 Ter	Revelganj, India	850	Bedload				0.511712	5	-17.9
Kosi River									
LO 762	Chatara, Nepal	180	Suspended Load	0.282155	6	-22.3	0.511714	5	-17.9
LO 762 re-run				0.282162	9	-22.0			
LO 763	Chatara, Nepal	180	Bank	0.282049	5	-26.0	0.511689	7	-18.4
LO 763 Dup	Chatara, Nepal	180	Bank	0.282040	7	-26.3			
PB 69	Chatara, Nepal	440	Suspended Load	0.282123	5	-23.4	0.511601	8	-20.1
PB 70	Chatara, Nepal	440	Bank	0.282064	9	-25.5	0.511649	8	-19.1
BR 331	Dumarighat, India	440	Bank	0.282136	7	-23.0	0.511656	7	-19.0
BR 332	Dumarighat, India	440	Bank	0.282125	6	-23.3	0.511722	9	-17.7
BR 332 re-run				0.282122	6	-23.5			
Narayani River									
LO 757	Narayanghat, Nepal	200	Suspended Load	0.282112	7	-23.8	0.511711	7	-17.9
LO 756	Narayanghat, Nepal	200	Suspended Load	0.282114	6	-23.7	0.511686	6	-18.4
LO 754	Narayanghat, Nepal	200	Suspended Load	0.282085	5	-24.7	0.511681	6	-18.5
LO 755	Narayanghat, Nepal	200	Suspended Load	0.282092	10	-24.5	0.511662	7	-18.9
LO 755 Dup	Narayanghat, Nepal	200	Suspended Load	0.282067	10	-25.4			
LO 758 C	Narayanghat, Nepal	200	Suspended Load	0.282135	4	-23.0	0.511661	5	-18.9
PB 54	Narayanghat, Nepal	200	Suspended Load	0.282055	7	-25.8	0.511661	5	-18.9
LO 1002	Narayanghat, Nepal	200	Suspended Load	0.282129	15	-23.2	0.511712	8	-17.9
LO 1002 re-run				0.282125	12	-23.3	0.511743	11	-17.3
LO 1007	Narayanghat, Nepal	200	Suspended Load	0.282007	12	-27.5	0.511655	13	-19.0
LO 1007 Dup	Narayanghat, Nepal	200	Suspended Load	0.282001	6	-27.7	0.511632	11	-19.5
BR 8106	Hajipur, India	550	Suspended Load	0.282149	6	-22.5	0.511633	6	-19.4
BR 8107	Hajipur, India	550	Bedload	0.282100	5	-24.2	0.511734	7	-17.5

Figure 1

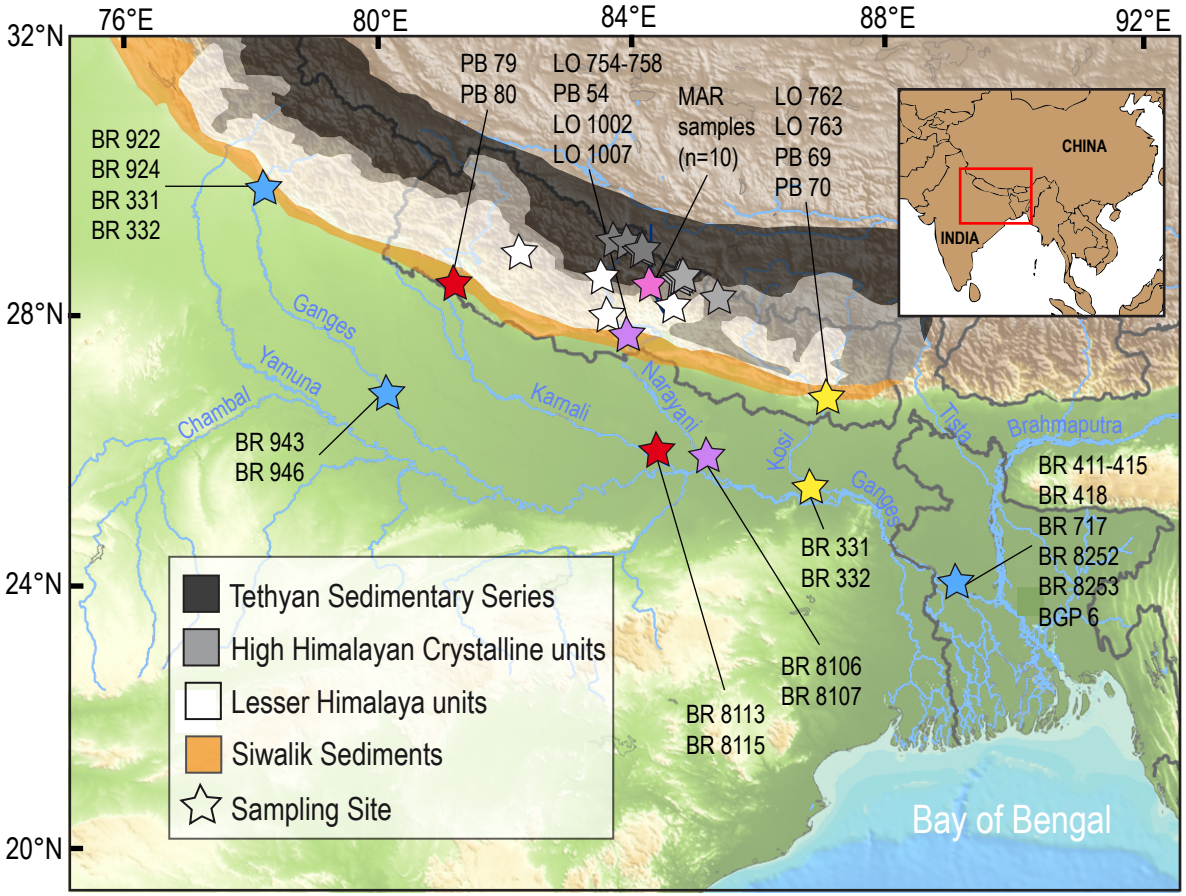
76°E
80°E
84°E
88°E
92°E
32°N
28°N
24°N
20°N
PB 79
PB 80
LO 754-758
PB 54
LO 1002
LO 1007
MAR
samples
(n=10)
LO 762
LO 763
PB 69
PB 70
BR 922
BR 924
BR 331
BR 332
CHINA
INDIA
Ganges
Yamuna
Chambal
Kamali
Narayani
Kosi
Tista
Brahmaputra
Ganges
BR 943
BR 946
BR 331
BR 332
BR 411-415
BR 418
BR 717
BR 8252
BR 8253
BGP 6
BR 8106
BR 8107
BR 8113
BR 8115
Tethyan Sedimentary Series
High Himalayan Crystalline units
Lesser Himalaya units
Siwalik Sediments
Sampling Site
Bay of Bengal

Figure 2

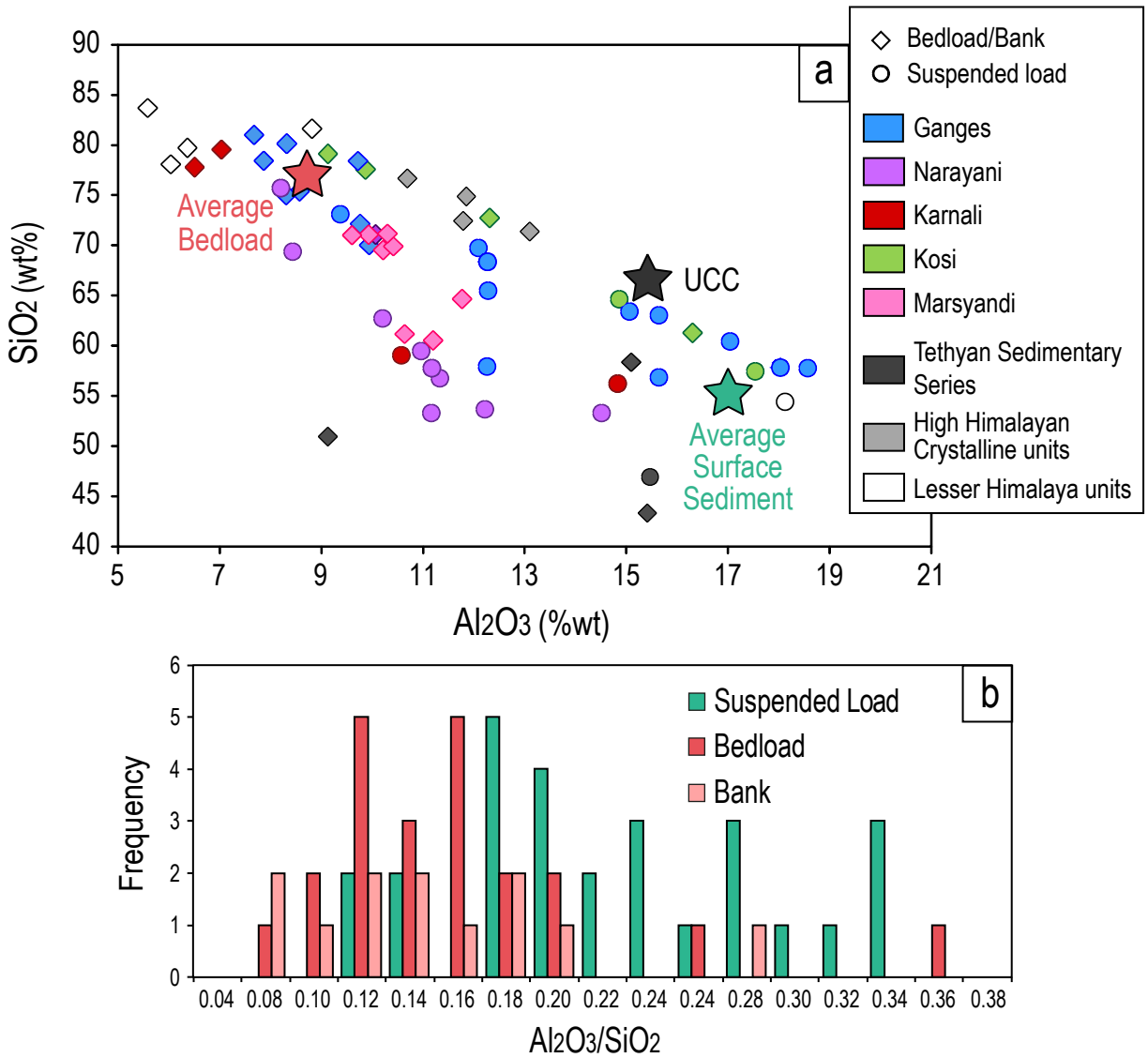
a
Bedload/Bank
Suspended load
Ganges
Narayani
Karnali
Kosi
Marsyandi
Tethyan Sedimentary Series
High Himalayan Crystalline units
Lesser Himalaya units
Average Bedload
UCC
Average Surface Sediment
SiO2 (wt%)
Al2O3 (%wt)
90
85
80
75
70
65
60
55
50
45
40
5
7
9
11
13
15
17
19
21
b
Suspended Load
Bedload
Bank
Frequency
0
1
2
3
4
5
6
0.04
0.08
0.10
0.12
0.14
0.16
0.18
0.20
0.22
0.24
0.24
0.28
0.30
0.32
0.34
0.36
0.38
Al2O3/SiO2

Figure 3

Figure 3

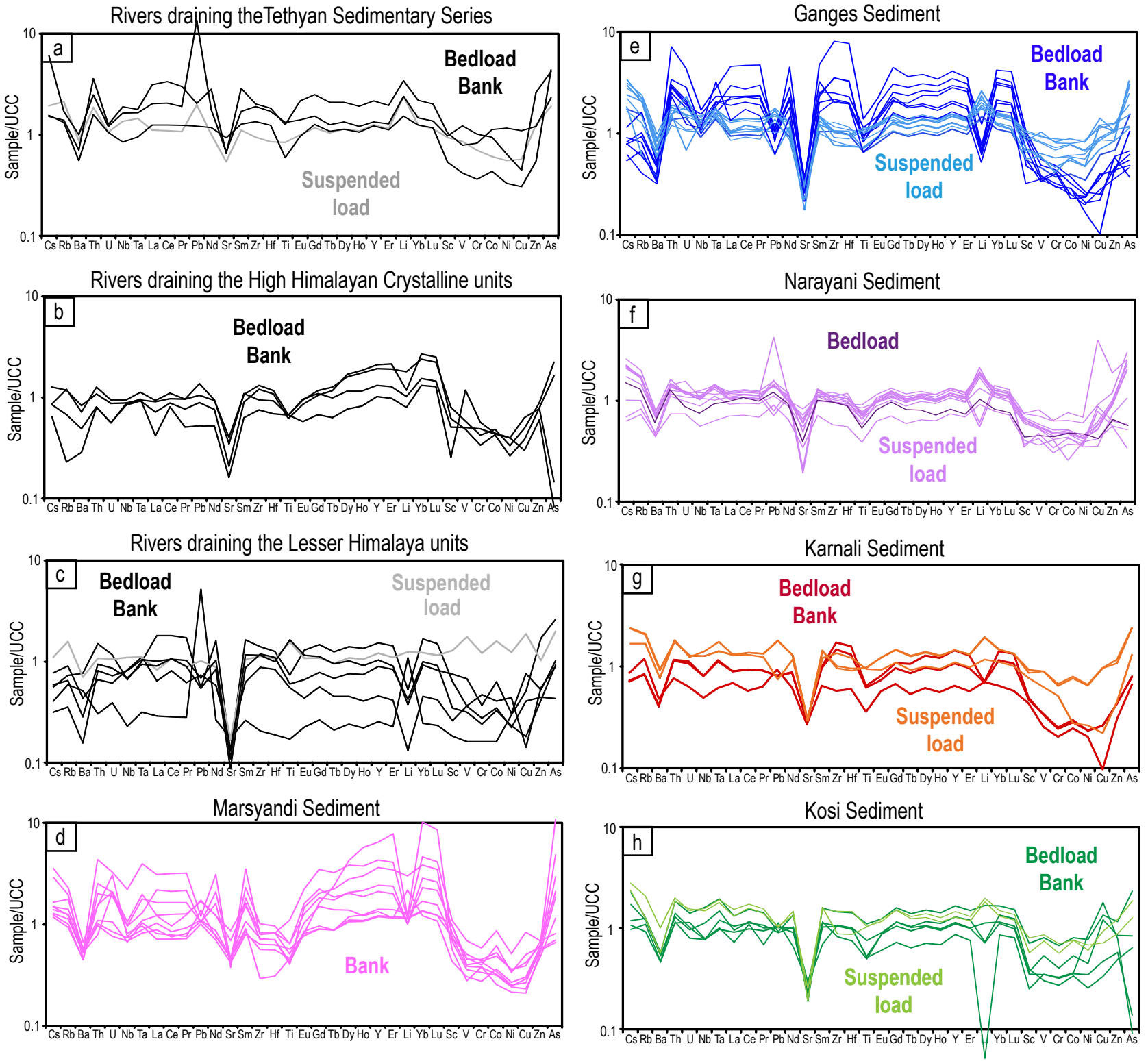

Figure 4

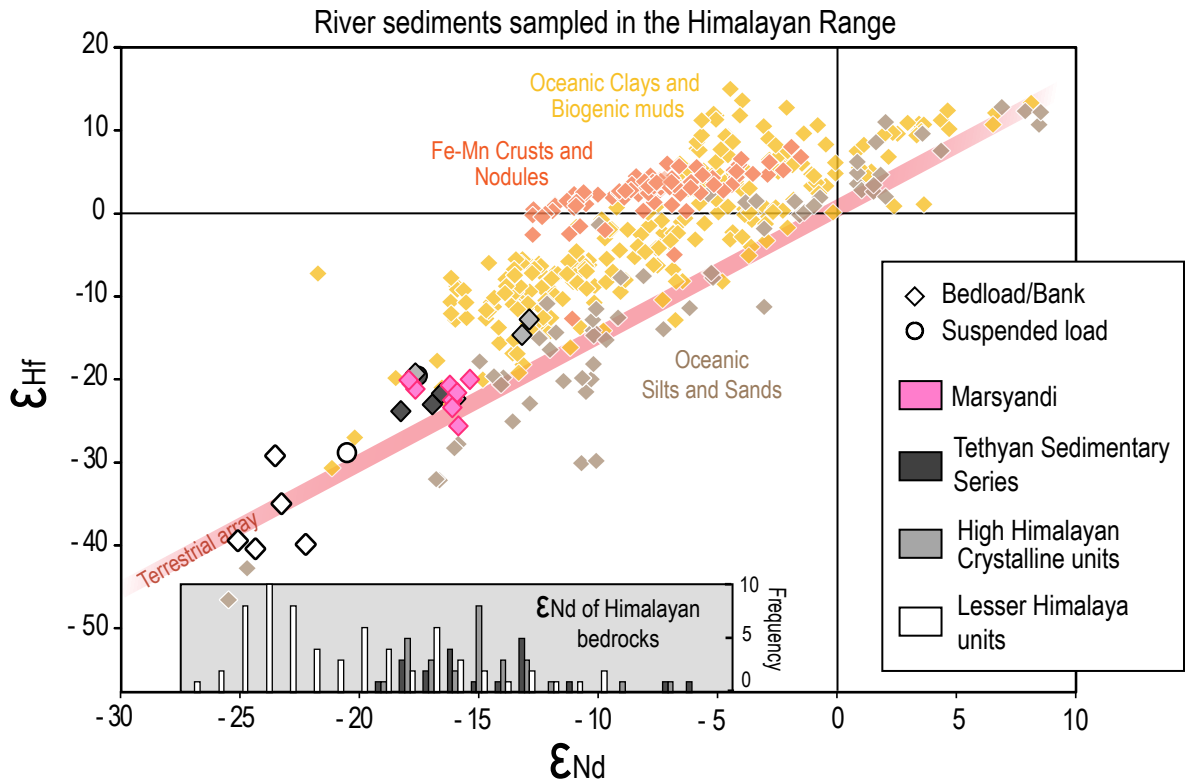
River sediments sampled in the Himalayan Range
Oceanic Clays and Biogenic muds
Fe-Mn Crusts and Nodules
Oceanic Silts and Sands
Terrestrial array
εNd of Himalayan bedrocks
Frequency
Bedload/Bank
Suspended load
Marsyandi
Tethyan Sedimentary Series
High Himalayan Crystalline units
Lesser Himalaya units
εHf
εNd
20
10
0
-10
-20
-30
-40
-50
-30
-25
-20
-15
-10
-5
0
5
10

Figure 5

Figure 5

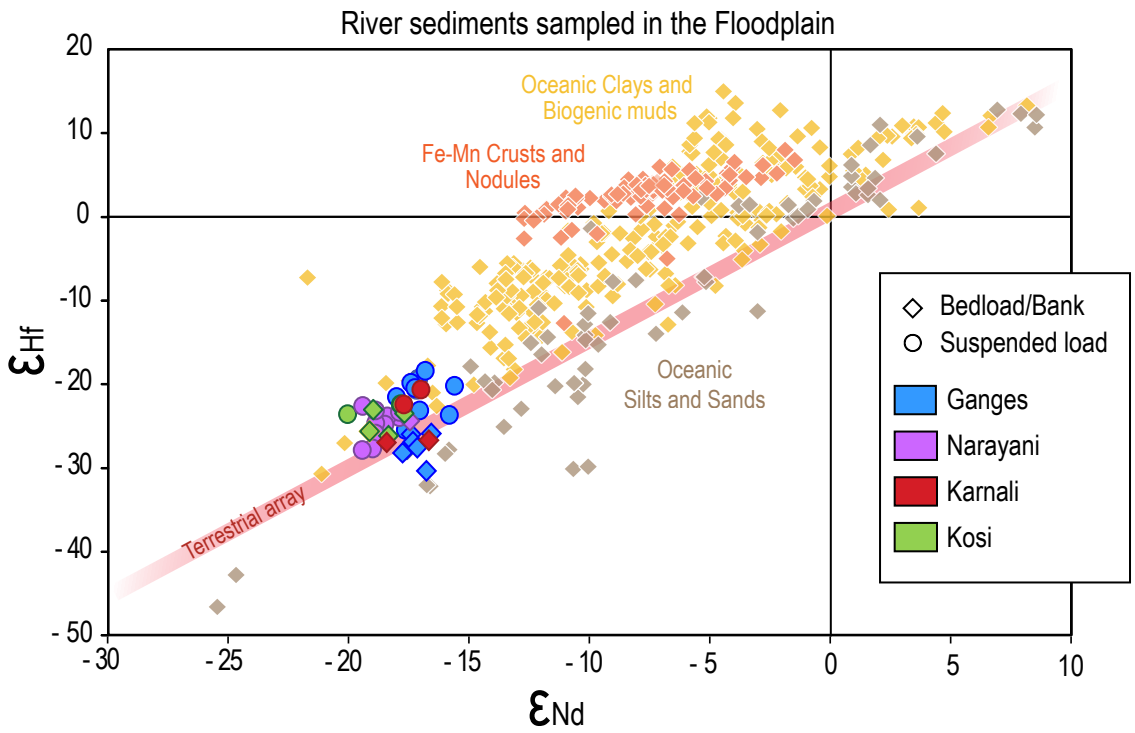

Figure 6

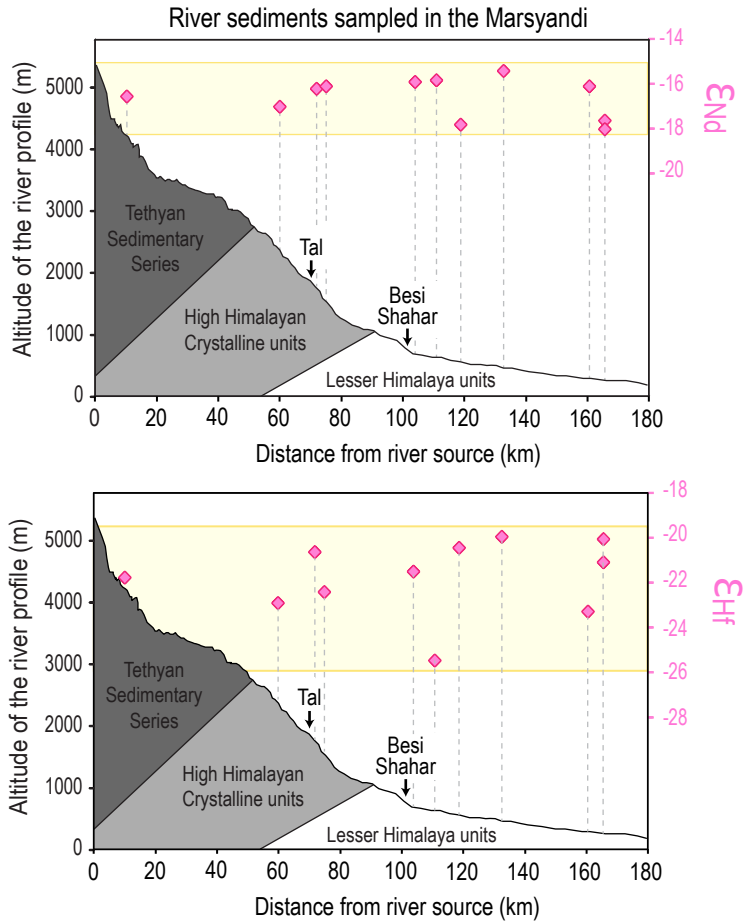
River sediments sampled in the Marsyandi
Altitude of the river profile (m)
Distance from river source (km)
Tethyan Sedimentary Series
High Himalayan Crystalline units
Lesser Himalaya units
Tal
Besi Shahar
εNd
εHf

Figure 7

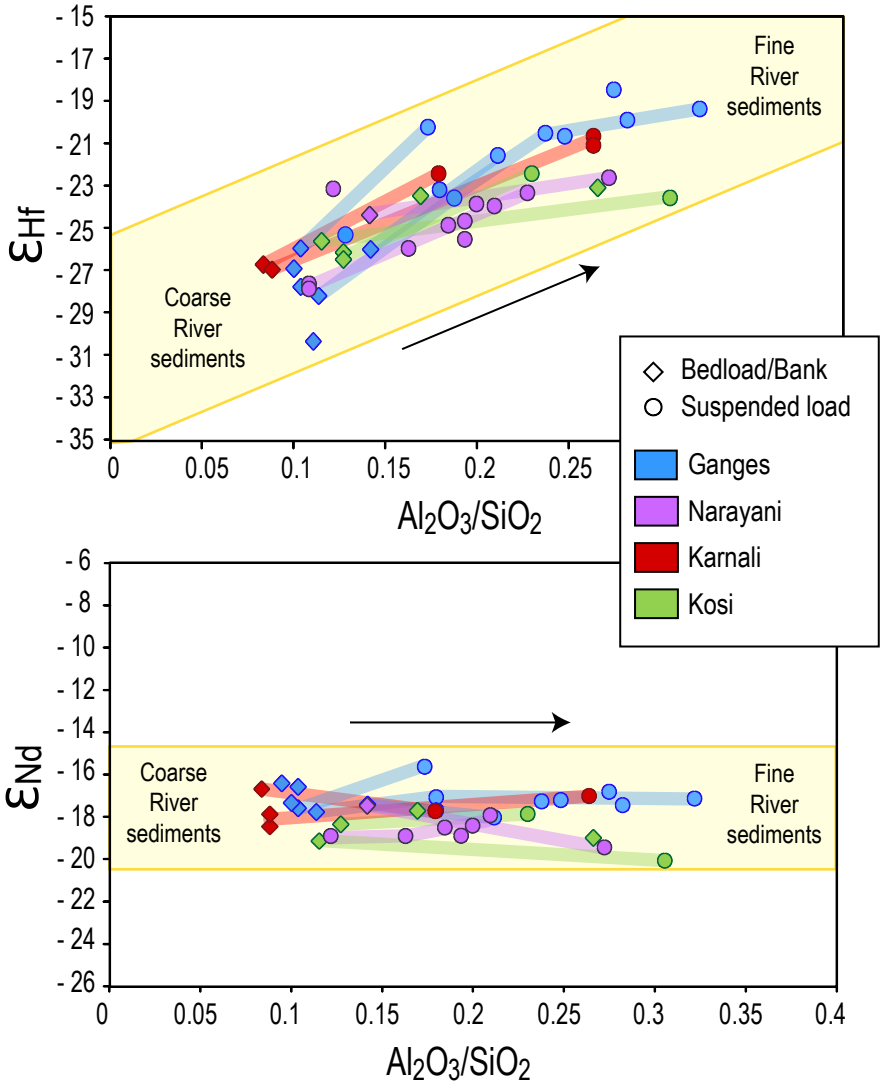
- 15
- 17
- 19
- 21
- 23
- 25
- 27
- 29
- 31
- 33
- 35
εHf
0
0.05
0.1
0.15
0.2
0.25
Al2O3/SiO2
Fine River sediments
Coarse River sediments
Bedload/Bank
Suspended load
Ganges
Narayani
Karnali
Kosi
- 6
- 8
- 10
- 12
- 14
- 16
- 18
- 20
- 22
- 24
- 26
εNd
0
0.05
0.1
0.15
0.2
0.25
0.3
0.35
0.4
Al2O3/SiO2
Coarse River sediments
Fine River sediments

Figure 8

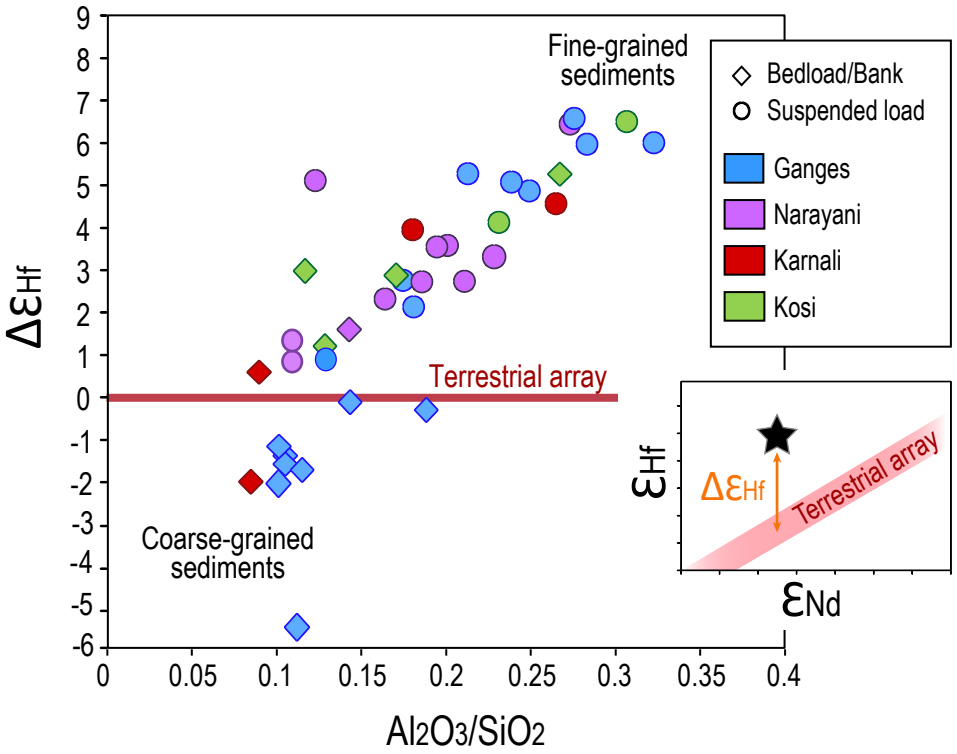
Fine-grained sediments
Coarse-grained sediments
Terrestrial array
Bedload/Bank
Suspended load
Ganges
Narayani
Karnali
Kosi
ΔεHf
Al2O3/SiO2
εHf
εNd
ΔεHf
Terrestrial array

Figure 9

Figure 9

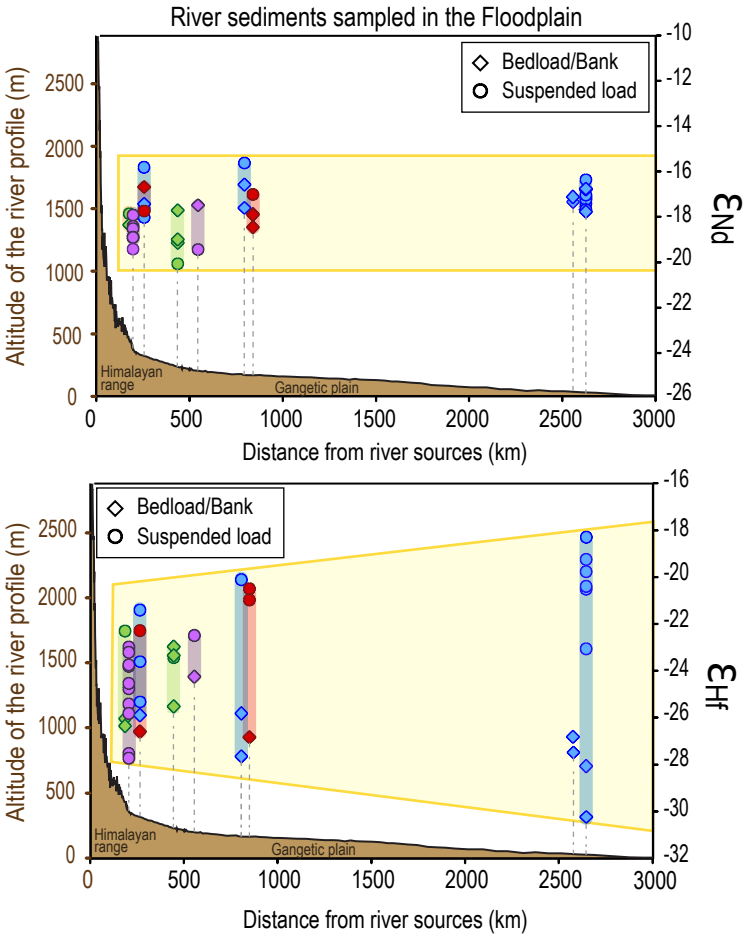

Figure 10

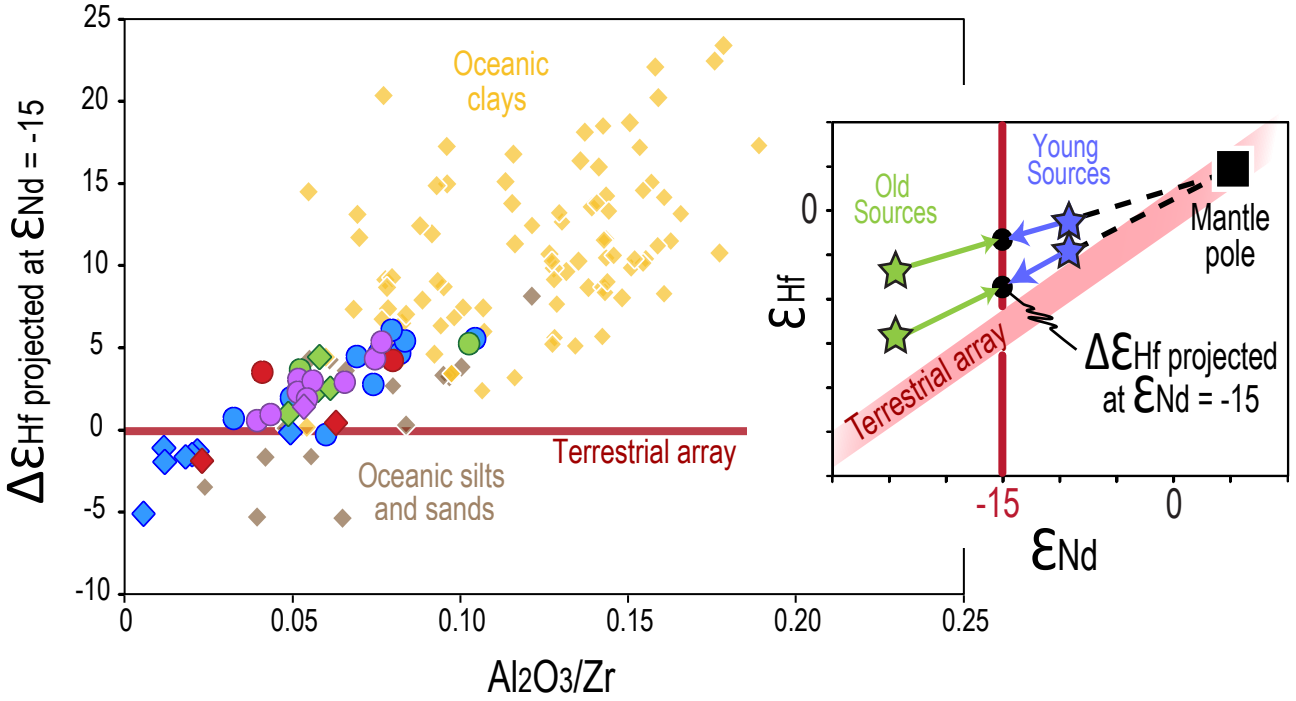
25
20
15
10
5
0
-5
-10
0
0.05
0.10
0.15
0.20
0.25
ΔεHf projected at εNd = -15
Al2O3/Zr
Oceanic clays
Terrestrial array
Oceanic silts and sands
Old Sources
Young Sources
Mantle pole
ΔεHf projected at εNd = -15
Terrestrial array
εHf
εNd
-15
0

Figure 11

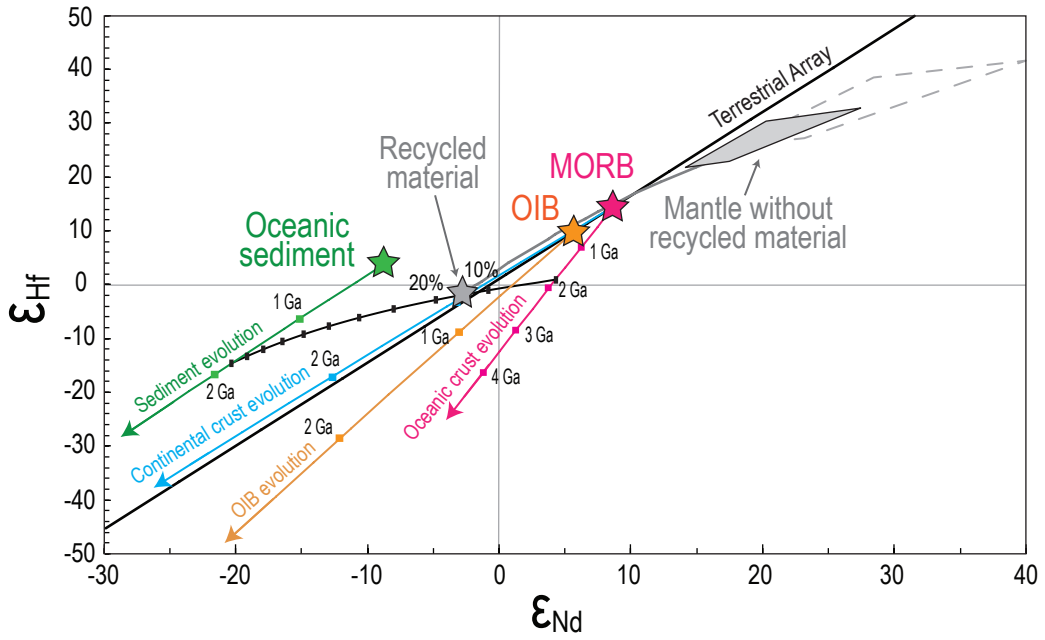
Figure 11
Terrestrial Array
Recycled material
MORB
OIB
Oceanic sediment
Mantle without recycled material
20%
10%
1 Ga
2 Ga
1 Ga
2 Ga
1 Ga
3 Ga
4 Ga
2 Ga
Sediment evolution
Continental crust evolution
Oceanic crust evolution
OIB evolution
εHf
εNd
50
40
30
20
10
0
-10
-20
-30
-40
-50
-30
-20
-10
0
10
20
30
40

Supplementary Table A: Weight mineral proportions in Ganga sediments modified after Garzanti et al. (2010, 2011)

Surface suspended loads (<3m)		
	Average	**2σ**
Quartz	34.3	22.8
K-feldspar	2.6	1.6
Albite	4.6	2.4
Ca-plagioclase	2.4	2.3
Lithic grain	ND	
Calcite	1.2	0.3
Dolomite	1.8	0.2
Muscovite	17.5	9.2
Biotite	10.4	4.3
Chlorite	2.8	1.4
Clay	19.5	18.6
Fe-oxides	0.2	0.2
Fibrolite	ND	
Opaques	1.3	0.1
Zircon	0.1	0.02
Tourmaline	0.2	0.1
Rutile	0.2	0.2
Ti oxide	0.4	0.1
Titanite	0.1	0.1
Apatite	0.1	0.04
Monazite	ND	
Amphibole	0.5	0.6
Pyroxene	0.2	0.1
Spinel	ND	
Epidote	1.4	0.8
Allanite	ND	
Chloritoid	ND	
Garnet	0.4	0.5
Staurolite	ND	
Kyanite	0.04	0.1
Sillimanite	ND	
Sum	*102.2*	

Deep suspended loads (>8m)		
	Average	**2σ**
Quartz	48.7	10.6
K-feldspar	5.7	2.3
Albite	5.9	4.0
Ca-plagioclase	4.2	2.8
Lithic grain	ND	
Calcite	2.9	1.6
Dolomite	2.3	2.1
Muscovite	8.9	5.4
Biotite	5.5	3.0
Chlorite	1.7	1.1
Clay	9.8	3.6
Fe-oxides	0.1	0.1
Fibrolite	ND	
Opaques	1.0	0.7
Zircon	0.1	0.3
Tourmaline	0.2	0.1
Rutile	0.2	0.2
Ti oxide	0.2	0.2
Titanite	0.2	0.3
Apatite	0.1	0.1
Monazite	ND	
Amphibole	1.1	0.6
Pyroxene	0.3	0.2
Spinel	ND	
Epidote	1.0	0.3
Allanite	0.02	0.1
Chloritoid	ND	
Garnet	1.2	1.9
Staurolite	0.03	0.02
Kyanite	0.1	0.1
Sillimanite	0.1	0.1
Sum	*101.4*	

Bedloads		
	Average	**2σ**
Quartz	55.4	14.9
K-Feldspar	6.6	3.1
Plagioclase	6.0	2.9
Lithic grain	14.5	5.2
Calcite	ND	
Dolomite	ND	
Micas	9.8	21.9
Chlorite	ND	
Clay	ND	
Fe-oxides	ND	
Fibrolite	0.1	0.2
Opaques	1.1	2.8
Zircon	0.1	0.4
Tourmaline	0.3	0.7
Rutile	0.1	0.2
Ti oxide	0.0	0.1
Titanite	0.3	0.5
Apatite	0.1	0.4
Monazite	0.1	0.3
Amphibole	1.4	2.0
Pyroxene	0.3	0.5
Cr-spinel	ND	
Epidote	1.0	1.5
Allanite	ND	
Chloritoid	ND	
Garnet	2.8	6.5
Staurolite	0.1	0.1
Kyanite	0.2	0.5
Sillimanite	0.02	0.1
Sum	*100.3*	

ND: not determined or under detection limit

Supplementary Table B: Major and Trace element concentrations in sediments from rivers draining monolithologic basins

Sample Name	R 94-12	MO 102	MO 112	PB 33	PB 37	MO 207	MO 73
Locality	Sarmi, Nepal	Confluence Darondi/Marsel Khola, Nepal	Confluence Bhuri Gandaki/Isul Khola, Nepal	Nepal	Nepal	Waling, Nepal	Nepal
Latitude	29.06	28.04111	28.04694	28.48966	28.43248	28.04288	28.25139
Longitude	82.50	84.66944	84.81472	83.65016	83.59952	83.79026	84.67278
River	Tributary of the Bheri River	Marsel Khola	Isul Khola	Ghara khola	Beg Khola	Andi Khola	Tributary of the Chepe khola
Sampling date	16-Mar-94	11-May-97	12-May-97	9-Jul-05	9-Jul-05	18-May-97	8-May-97
Drained lithology	Lesser Himalaya	Lesser Himalaya	Lesser Himalaya	Lesser Himalaya	Lesser Himalaya	Lesser Himalaya	High Himalayan Crystalline
Type of sediment	Bedload	Bank	Bank, gravel sample	Suspended Load	Bank	Bedload	Bank
Sampling Depth (m)				0			
ppm							
Cs	1.97	3.75	2.73	5.37	1.53	2.86	3.18
Rb	48.8	74.9	60.6	131	29.6	53.9	19.5
Ba	318	269	475	438	97.0	176	181
Th	3.14	6.91	15.6	11.3	8.45	9.77	8.41
U	1.05	1.64	3.13	2.82	1.93	2.30	1.53
Nb	2.72	9.83	7.89	13.0	9.61	8.19	10.4
Ta	0.281	0.987	0.893	0.986	0.933	0.837	0.872
La	8.83	19.7	55.3	25.5	30.9	27.7	13.1
Ce	17.6	50.5	113	66.5	65.7	66.7	50.8
Pr	1.97	4.36	12.1	6.21	7.25	6.31	3.62
Pb	87.1	12.4	9.19	17.1	11.6	9.12	8.94
Nd	7.08	15.6	42.9	23.5	27.5	22.3	14.1
Sr	55.0	53.0	41.1	53.8	34.3	27.4	52.1
Sm	1.22	2.90	7.66	4.86	5.41	4.05	2.99
Zr	39.1	168	268	216	220	227	146
Hf	0.982	4.39	6.62	5.58	5.22	5.76	3.68
Ti	649	2088	2810	5960	6246	2279	2584
Eu	0.223	0.431	1.28	1.06	1.15	0.653	0.581
Gd	1.04	2.21	5.84	4.29	4.42	3.10	2.71
Tb	0.145	0.313	0.865	0.667	0.658	0.472	0.446
Dy	0.928	1.74	5.42	4.22	3.92	2.92	3.02
Ho	0.181	0.333	1.10	0.872	0.751	0.614	0.683
Y	5.26	9.47	31.8	25.2	21.6	18.5	21.5
Er	0.516	0.943	3.27	2.51	2.06	1.90	2.26
Li	25.9	3.15	12.6	29.7	8.90	10.1	19.3
Yb	0.473	0.879	3.24	2.38	1.78	1.94	2.58
Lu	0.0718	0.128	0.463	0.355	0.253	0.281	0.397
Sc	2.53	3.6	8.79	17.8	10.4	4.81	3.60
V	15.4	35.1	34.6	168	65.1	30.3	114
Cr	14.7	43.0	25.0	111	33.5	21.9	52.2
Co	2.74	6.96	5.92	27.2	10.8	5.63	7.71
Ni	13.8	20.3	10.3	57.5	14.2	10.8	18.9
Cu	14.0	3.91	11.3	52.0	21.0	4.99	8.50
Zn	113	36.5	29.3	68.4	34.6	27.6	40.3
As	12.4	4.25	2.04	9.47	4.85	4.37	0.404
wt.%							
SiO2	22.24	81.82	79.89	54.44	83.90	78.27	76.81
Al2O3	2.78	8.82	6.36	18.12	5.59	6.04	10.69
Fe2O3	1.02	2.98	3.88	9.81	4.06	2.66	4.27
MnO	0.03	0.00	0.08	0.09	0.13	0.06	0.08
MgO	15.31	1.25	1.74	4.66	1.25	2.46	1.34
CaO	21.69	0.02	2.41	1.74	1.03	2.49	1.50
Na2O	0.04	0.82	0.68	1.25	1.13	0.16	1.20
K2O	1.33	1.96	1.40	3.46	0.64	2.19	1.93
TiO2	0.09	0.33	0.50	1.06	1.03	0.39	0.47
P2O5	0.10	0.08	0.11	0.15	0.10	0.13	0.12
LOI	35.10	1.80	2.80	5.65	1.30	5.15	1.53
Total	99.78	99.89	99.85	100.42	100.16	100.00	99.94

Sample Name	MO 50	MO 59	KN 83	MO 504	NAG 22	MAR-50	MAR-40
Locality	Nepal	Nepal	Ghyangphedi, Nepal	Tukche, Nepal	Pedi, Nepal	Temang, Nepal	Sabche, Nepal
Latitude	28.30056	28.29528	28.008	28.71120	28.78623	28.53000	28.63327
Longitude	84.63722	84.64639	85.454	83.64120	83.96370	84.31667	84.10613
River	Chepe khola	Chepe khola	Tadi khola	Yamkim khola	Marsyandi	Marsyandi	Sabche khola
Sampling date	6-May-97	7-May-97	21-Mar-94		28-Nov-95	15-Nov-00	12-Nov-00
Drained lithology	High Himalayan Crystalline	High Himalayan Crystalline	High Himalayan Crystalline	Tethys Himalaya	Tethys Himalaya	Tethys Himalaya	Tethys Himalaya
Type of sediment	Bank	Bank	Bedload	Suspended Load	Bedload	Bedload	Bedload
Sampling Depth (m)				0			
ppm							
Cs	4.16	6.21	4.24	9.58	30.5	7.72	7.52
Rb	56.9	99.6	101	180	144	113	118
Ba	310	524	452	553	633	351	447
Th	8.49	11.4	13.3	19.7	26.4	16.7	38.2
U	1.52	2.36	2.56	2.9	3.29	2.87	3.45
Nb	10.1	10.6	11.4	16.4	19.8	10.2	23.0
Ta	0.839	0.853	1.01	1.32	1.50	0.862	1.62
La	22.4	28.3	29.0	34.6	63.4	39.0	98.4
Ce	55.5	61.1	69.4	69.7	131	79.2	215
Pr	5.48	6.85	6.86	7.72	13.6	8.86	21.6
Pb	15.1	23.3	17.9	33.9	235	20.9	35.2
Nd	20.7	25.5	25.2	27.4	48.2	32.1	77.3
Sr	67.2	111	130	174	217	301	211
Sm	4.22	5.14	5.03	5.27	8.09	6.02	13.7
Zr	233	183	255	183	370	263	393
Hf	5.74	4.91	6.21	4.54	9.12	6.65	9.77
Ti	2385	2581	2588	3254	5117	2288	4862
Eu	0.856	0.948	0.966	1.00	1.42	0.971	2.19
Gd	4.22	4.70	4.39	4.71	6.15	5.12	10.1
Tb	0.824	0.888	0.694	0.733	0.889	0.764	1.48
Dy	6.61	6.28	4.52	4.49	5.28	4.45	8.25
Ho	1.55	1.45	0.963	0.911	1.01	0.888	1.60
Y	44.4	40.3	27.7	26.7	28.3	25.9	46.0
Er	4.94	4.38	2.94	2.66	2.98	2.59	4.55
Li	28.5	43.2	24.6	57.8	58.2	37.1	83.5
Yb	5.27	4.70	3.02	2.47	2.90	2.48	4.35
Lu	0.78	0.695	0.452	0.359	0.427	0.366	0.63
Sc	8.70	11.2	7.2	13.3	13.8	7.53	14.7
V	47.4	56.7	49.1	83.7	120	40.7	77.1
Cr	31.2	39.1	45.3	65.0	93.9	33.5	76.3
Co	7.41	8.45	7.56	10.6	16.5	7.54	19.6
Ni	12.6	15.9	18.9	26.3	30.5	15.6	55.3
Cu	10.8	13.9	17.7	16.0	12.5	8.59	30.9
Zn	53.0	59.6	52.2	85.6	179	36.6	81.9
As	7.84	10.8	0.712	9.26	20.5	21.3	11.3
wt.%							
SiO2	72.56	71.52	75.02	46.94	43.33	50.97	58.44
Al2O3	11.79	13.10	11.85	15.46	15.41	9.13	15.10
Fe2O3	6.04	5.36	3.76	5.14	5.60	2.95	6.13
MnO	0.27	0.19	0.07	0.05	0.04	0.03	0.04
MgO	1.01	1.48	1.05	2.66	2.10	1.58	0.61
CaO	1.18	1.35	1.39	11.19	13.07	17.24	6.24
Na2O	1.51	1.87	1.57	0.55	0.51	1.46	0.85
K2O	1.73	2.37	2.50	4.22	3.72	2.31	2.79
TiO2	0.42	0.47	0.45	0.56	0.80	0.38	0.73
P2O5	0.11	0.16	0.08	0.20	0.16	0.06	0.17
LOI	1.55	2.08	1.26	12.74	14.95	13.42	9.02
Total	98.17	99.95	98.99	99.71	99.69	99.53	100.12

Supplementary Table A: Major and Trace element concentrations in sediments from the Ganga and its major tributaries and the Marsyandi River

Sample Name	BR 931	BR 932	BR 922*	BR 924*	BR 943*	BR 946*	BR 946 Dup
Locality	Devrapayag, India	Devrapayag, India	Rishikesh, India	Rishikesh, India	Kanpur, India	Kanpur, India	Kanpur, India
Latitude			30.12661	30.12661	26.61306	26.61306	26.61306
Longitude			78.33044	78.33044	80.27576	80.27576	80.27576
River	Ganga	Ganga	Ganga	Ganga	Ganga	Ganga	Ganga
Sampling date	12-Aug-09	12-Aug-09	11-Aug-09	11-Aug-09	18-Aug-09	18-Aug-09	18-Aug-09
Type of sediment	Suspended Load	Suspended Load	Suspended Load	Bank	Suspended Load	Bedload	Bedload
Sampling Depth (m)	0	0	0.2		1.7		
Cs	16.4	8.00	14.6	8.47	10.8	5.61	4.44
Rb	185	115	170	128	125	136	68.4
Ba	469	344	436	368	391	328	221
Th	16.1	20.7	16.3	14.4	12.6	35.4	26.3
U	6.24	5.75	4.93	3.83	2.89	7.64	4.76
Nb	13.6	11.0	13.6	11.0	12.6	13.9	15.5
Ta	1.58	1.13	1.60	1.24	1.30	1.65	1.83
La	31.6	44.6	32.5	29.2	26.6	91.1	58.4
Ce	66.1	90.1	69.9	61.4	58.5	170	128
Pr	7.56	10.3	7.65	6.75	6.28	21.2	13.5
Pb	29.2	21.0	29.1	21.4	23.5	18.9	15.8
Nd	27.7	37.2	28.0	25.0	23.5	76.6	48.3
Sr	88.8	90.9	86.5	97.4	71.5	107	69.0
Sm	5.81	7.18	5.77	4.87	4.74	15.1	9.45
Zr	205	290	150	202	163	388	417
Hf	5.59	8.23	3.96	5.20	4.07	10.3	10.6
Ti	2750	2619	2836	2510	2841	3407	3675
Eu	0.916	0.972	0.942	0.813	0.891	1.94	1.16
Gd	5.22	5.87	5.14	4.16	4.26	12.1	8.19
Tb	0.868	0.888	0.789	0.653	0.678	1.98	1.39
Dy	5.44	5.06	4.73	3.96	4.25	12.0	9.20
Ho	1.10	1.00	0.926	0.784	0.846	2.42	1.94
Y	32.5	29.1	26.8	23.0	24.9	72.5	58.8
Er	3.16	2.90	2.62	2.25	2.47	7.05	5.88
Li	62.9	31.5	56.5	35.2	43.8	29.6	18.4
Yb	3.03	2.83	2.47	2.15	2.38	6.83	5.92
Lu	0.449	0.428	0.344	0.315	0.339	0.993	0.869
Sc	10.1	8.72	7.93	7.61	9.55	12.3	6.65
V	56.4	43.4	58.3	44.5	62.1	36.8	37.0
Cr	43.3	32.4	38.3	34.2	53.3	27.1	29.5
Co	9.52	7.66	10.0	6.87	10.6	5.01	4.94
Ni	22.5	14.7	22.5	16.3	29.5	7.70	9.82
Cu	19.7	14.4	33.6	17.2	25.3	2.86	6.15
Zn	56.4	41.9	70.7	46.0	68.9	31.1	39.8
As	15.8	9.01	13.5	7.43	11.9	3.00	3.22
wt.%							
SiO2	65.51	73.12	57.94	70.03	69.75	80.14	
Al2O3	12.28	9.37	12.26	9.95	12.09	8.32	
Fe2O3	4.01	3.19	4.40	3.15	4.51	3.59	
MnO	0.07	0.06	0.07	0.05	0.07	0.15	
MgO	2.99	2.24	4.98	2.64	2.09	1.01	
CaO	4.12	3.54	6.11	3.94	1.78	1.80	
Na2O	1.75	1.56	1.46	1.60	1.23	1.41	
K2O	3.25	2.27	3.20	2.57	2.82	1.51	
TiO2	0.48	0.44	0.50	0.42	0.50	0.63	
P2O5	0.13	0.12	0.14	0.11	0.14	0.23	
LOI	6.35	4.60		4.96		1.38	
Total	100.94	100.51	91.06	99.42	94.96	100.16	

* Major element concentrations already published in Lupker et al. (2012)
** Major element conceentrations alreary published in Galy and France-Lanord (2001)

Sample Name	BGP 6**	BGP 6 Dup	BR 415*	BR 414*	BR 413*	BR 412*	BR 411*
Locality	Rajshahi, India	Rajshahi, India	Harding bridge, Bangladesh	Harding bridge, Bangladesh	Harding bridge, Bangladesh	Harding bridge, Bangladesh	Harding bridge, Bangladesh
Latitude	24.35833	24.35833	24.05290	24.05290	24.05290	24.05290	24.05290
Longitude	88.60833	88.60833	89.02465	89.02465	89.02465	89.02465	89.02465
River	Ganga	Ganga	Ganga	Ganga	Ganga	Ganga	Ganga
Sampling date	2-Aug-93	2-Aug-93	13-Jul-04	13-Jul-04	13-Jul-04	13-Jul-04	13-Jul-04
Type of sediment	Bedload	Bedload	Suspended Load	Suspended Load	Suspended Load	Suspended Load	Suspended Load
Sampling Depth (m)			0	2	4	6.5	9
Cs	3.83	4.02	15.4	13.6	11.8	11.7	8.08
Rb	77.9	85.2	202	186	174	175	107
Ba	294	307	627	562	531	527	372
Th	30.2	31.3	20.0	19.0	19.3	18.0	15.1
U	5.41	5.71	4.64	4.08	4.15	3.96	2.92
Nb	12.9	12.0	17.4	17.9	16.5	15.7	13.6
Ta	1.78	1.44	1.54	1.57	1.45	1.39	1.37
La	67.1	70.2	42.0	41.3	42.2	40.0	32.8
Ce	144	145	89.4	88.1	89.2	84.7	76.3
Pr	15.5	16.4	9.75	9.77	9.87	9.29	7.84
Pb	17.8	17.6	30.4	26.2	25.3	25.3	17.4
Nd	56.5	60.8	35.0	35.7	35.8	34.0	29.0
Sr	115	117	84.1	91.0	99.3	101	88.6
Sm	10.9	11.4	6.93	6.98	7.01	6.77	5.60
Zr	683	667	178	204	227	199	249
Hf	17.1	17.4	4.73	5.22	5.79	5.17	6.14
Ti	3155	3166	4137	4198	3976	3833	3314
Eu	1.39	1.45	1.27	1.26	1.23	1.20	1.04
Gd	8.51	9.10	6.19	6.15	6.05	5.80	4.96
Tb	1.25	1.29	0.984	0.945	0.93	0.872	0.782
Dy	7.24	7.61	5.97	5.74	5.72	5.42	4.81
Ho	1.39	1.48	1.17	1.15	1.13	1.06	0.95
Y	41.1	43.5	32.7	32.8	32.5	30.9	27.1
Er	3.99	4.24	3.33	3.30	3.21	3.07	2.65
Li	14.7	16.3	51.8	48.2	43.5	41.9	32.2
Yb	3.87	4.16	3.18	3.11	3.06	2.88	2.51
Lu	0.587	0.614	0.461	0.45	0.448	0.417	0.366
Sc	7.74	9.81	15.0	14.4	13.5	12.8	9.04
V	32.7	34.8	93.4	90.7	81.1	79.1	61.8
Cr	36.9	38.4	76.6	81.9	67.0	63.4	53.4
Co	3.93	4.32	15.5	15.1	13.6	13.4	10.3
Ni	11.0	11.3	38.6	40.5	32.4	31.5	26.4
Cu	10.9	11.3	33.9	31.7	25.7	23.7	24.3
Zn	29.1	28.1	84.9	83.5	73.3	72.1	56.6
As	2.32	5.03	9.17	7.33	5.52	5.70	5.41
wt.%							
SiO2	78.45		57.76	60.42	63.07	63.44	68.36
Al2O3	7.86		18.57	17.04	15.64	15.06	12.27
Fe2O3	2.46		6.61	6.31	5.75	5.55	4.20
MnO	0.05		0.08	0.08	0.07	0.07	0.06
MgO	0.91		2.39	2.34	2.20	2.07	1.71
CaO	3.28		1.79	2.36	2.73	2.67	2.77
Na2O	1.48		1.03	1.13	1.19	1.22	1.37
K2O	1.83		3.77	3.52	3.28	3.20	2.82
TiO2	0.57		0.75	0.76	0.72	0.70	0.58
P2O5	0.12		0.16	0.15	0.15	0.14	0.12
LOI	2.57		7.19	6.51	6.07	6.13	4.66
Total	99.57		100.09	100.62	100.87	100.23	98.89

Sample Name	BR 418*	BR 8252*	BR 8253*	BR 717*	PB 79*	PB 80*	PB 80 Dup
Locality	Harding bridge, Bangladesh	Harding bridge, Bangladesh	Harding bridge, Bangladesh	Harding bridge, Bangladesh	Chisapani, Nepal	Chisapani, Nepal	Chisapani, Nepal
Latitude	24.05290	24.05290	24.05290	24.05290	28.63895	28.63895	28.63895
Longitude	89.02465	89.02465	89.02465	89.02465	81.28278	81.28278	81.28278
River	Ganga	Ganga	Ganga	Ganga	Kamali	Kamali	Kamali
Sampling date	13-Jul-04	10-Sep-08	10-Sep-08	17-Aug-07	15-Jul-05	15-Jul-05	15-Jul-05
Type of sediment	Bedload	Bedload	Suspended Load	Bedload	Suspended Load	Bank	Bank
Sampling Depth (m)	10	14	0	11	0		
Cs	2.64	3.05	8.92	3.87	8.20	3.50	3.56
Rb	56.6	34.5	51.7	50.3	141	70.7	71.2
Ba	212	203	240	244	482	255	262
Th	29.7	24.3	16.1	74.2	19.0	12.0	12.3
U	5.14	3.33	1.85	11.7	3.33	2.92	3.07
Nb	18.4	13.6	15.8	20.3	16.9	9.79	9.79
Ta	2.08	2.91	1.31	2.50	1.57	1.04	1.01
La	71.0	41.6	30.8	141	39.8	27.9	27.9
Ce	146	110	75.4	292	82.0	59.7	59.2
Pr	16.7	10.6	8.12	33.1	8.78	6.52	6.55
Pb	15.0	10.7	10.5	14.2	12.7	13.9	14.0
Nd	60.4	39.4	31.2	121	31.6	23.7	23.9
Sr	103	83.6	56.5	98.3	96.3	93.8	94.5
Sm	12.0	7.63	6.27	22.3	5.69	4.55	4.70
Zr	479	403	196	1550	259	285	337
Hf	12.1	10.5	5.13	40.5	6.43	7.03	8.49
Ti	4355	2523	4323	5299	3606	2395	2485
Eu	1.48	0.928	1.19	2.24	0.927	0.74	0.817
Gd	10.1	6.41	5.44	17.7	4.37	3.90	4.38
Tb	1.64	0.977	0.854	2.52	0.644	0.603	0.746
Dy	10.3	5.70	5.32	14.7	3.90	3.84	5.02
Ho	2.12	1.16	1.06	2.83	0.787	0.776	1.02
Y	62.0	34.5	31.1	85.6	23.0	22.6	30.5
Er	6.35	3.33	3.04	8.11	2.26	2.24	2.97
Li	15.8	12.6	45.3	15.7	28.1	16.9	17.0
Yb	6.23	3.32	2.95	8.17	2.18	2.28	2.79
Lu	0.905	0.50	0.433	1.25	0.312	0.333	0.416
Sc	13.2	4.56	11.8	14.3	10.7	6.63	6.95
V	46.9	34.5	100	53.5	60.6	33.0	32.4
Cr	40.0	28.2	73.6	44.1	47.2	23.2	22.3
Co	5.58	4.46	13.8	6.40	4.77	5.15	4.89
Ni	11.7	9.39	39.4	12.4	12.4	11.0	11.0
Cu	10.0	7.82	39.4	7.10	6.19	7.33	7.38
Zn	38.8	24.2	70.4	31.0	30.2	29.2	29.1
As	1.79	2.21	14.6	2.63	6.24	3.80	3.85
wt.%							
SiO2	75.40	80.96	56.94	75.03	59.03	77.77	
Al2O3	8.58	7.68	15.64	8.31	10.57	6.50	
Fe2O3	5.19	2.57	6.31	4.53	3.94	2.57	
MnO	0.19	0.06	0.09	0.13	0.06	0.05	
MgO	1.47	0.90	2.74	1.17	3.46	1.42	
CaO	4.15	2.50	4.25	3.29	8.69	4.56	
Na2O	1.18	1.41	0.97	1.29	1.15	0.92	
K2O	1.26	1.74	3.28	1.72	2.75	1.56	
TiO2	0.91	0.47	0.75	0.90	0.51	0.45	
P2O5	0.27	0.10	0.14	0.19	0.12	0.10	
LOI	2.15	2.19	8.93	2.65	10.51	4.58	
Total	100.73	100.58	100.04	99.18	100.79	100.49	

Sample Name	BR 8113*	BR 8113 Dup	BR 8115*	LO 762*	LO 763*	LO 763 Dup	PB 69*
Locality	Revelganj, India	Revelganj, India	Revelganj, India	Chatara, Nepal	Chatara, Nepal	Chatara, Nepal	Chatara, Nepal
Latitude	25.77950	25.77950	25.77950	26.84815	26.84815	26.84815	26.84815
Longitude	84.63070	84.63070	84.63070	87.15137	87.15137	87.15137	87.15137
River	Kamali	Kamali	Kamali	Kosi	Kosi	Kosi	Kosi
Sampling date	18-Aug-08	18-Aug-08	18-Aug-08	16-Aug-07	16-Aug-07	16-Aug-07	13-Jul-05
Type of sediment	Suspended Load	Suspended Load	Bedload	Suspended Load	Bank	Bank	Suspended Load
Sampling Depth (m)	0	0	5.4	0			0
Cs	11.5	11.7	4.31	11.6	5.26	5.84	13.8
Rb	173	176	101	107	77.2	106	177
Ba	574	586	305	357	290	341	637
Th	18.5	18.4	8.06	19.5	12.1	11.8	21.0
U	3.42	3.47	1.72	4.23	2.15	3.08	4.06
Nb	15.2	15.2	5.94	17.9	9.23	9.48	18.9
Ta	1.28	1.27	0.554	1.63	0.878	0.902	1.73
La	39.9	40.5	21.5	40.9	28.3	22.3	48.0
Ce	86.0	86.3	36.5	101	61.7	68.5	109
Pr	9.43	9.53	4.55	9.92	6.70	4.86	11.2
Pb	30.3	30.5	16.0	17.8	17.6	19.1	17.3
Nd	34.7	34.7	16.8	36.4	24.3	17.7	40.0
Sr	93.5	93.8	86.3	82.2	74.2	88.7	61.9
Sm	6.72	6.65	3.07	7.25	4.80	3.28	7.60
Zr	186	195	112	286	203	206	171
Hf	4.81	5.07	3.20	7.79	5.17	5.30	4.62
Ti	3763	3708	1382	4017	2013	1961	3979
Eu	1.23	1.23	0.576	1.17	0.872	0.601	1.24
Gd	5.78	5.85	2.70	6.15	4.21	2.88	6.03
Tb	0.88	0.891	0.376	0.92	0.658	0.447	0.875
Dy	5.33	5.43	2.40	5.45	4.03	2.76	5.00
Ho	1.05	1.07	0.468	1.06	0.79	0.571	0.969
Y	30.3	30.3	13.7	30.8	23.2	18.2	27.2
Er	2.99	3.03	1.32	3.02	2.29	1.73	2.73
Li	46.5	46.7	17.0	47.9	17.2	1.23	44.0
Yb	2.85	2.89	1.27	2.94	2.18	1.67	2.60
Lu	0.413	0.413	0.179	0.426	0.305	0.25	0.374
Sc	12.1	13.0	6.08	8.04	4.90	3.49	11.3
V	87.1	86.7	24.8	73.2	33.7	33.7	83.9
Cr	59.3	61.9	18.6	52.1	29.9	29.1	65.2
Co	13.2	13.8	4.25	13.2	6.20	6.10	13.3
Ni	30.5	31.0	9.55	28.6	40.4	16.3	32.2
Cu	26.8	27.1	2.72	26.4	50.2	13.2	20.2
Zn	71.9	78.6	20.5	83.2	52.8	38.5	59.6
As	11.4	11.5	3.24	9.01	0.434	0.651	6.17
wt.%							
SiO2	56.24		79.56	64.64	77.58		57.44
Al2O3	14.83		7.03	14.86	9.87		17.54
Fe2O3	5.75		1.72	5.34	2.92		6.00
MnO	0.08		0.03	0.07	0.04		0.07
MgO	3.26		1.17	2.15	1.20		3.78
CaO	4.80		3.41	1.88	1.58		2.24
Na2O	0.87		1.22	1.78	1.72		1.59
K2O	3.50		1.87	3.61	2.35		4.52
TiO2	0.65		0.24	0.68	0.38		0.73
P2O5	0.13		0.06	0.17	0.11		0.15
LOI	9.56		3.79	3.80	1.95		5.83
Total	99.67		100.08	98.98	99.68		99.91

Sample Name	PB 70*	BR 331*	BR 332*	LO 757*	LO 756*	LO 754*	LO 755*
Locality	Chatara, Nepal	Dumarighat, India	Dumarighat, India	Narayanghat, Nepal	Narayanghat, Nepal	Narayanghat, Nepal	Narayanghat, Nepal
Latitude	26.84815	25.54113	25.54113	27.70297	27.70297	27.70297	27.70297
Longitude	87.15137	86.72231	86.72231	84.42661	84.42661	84.42661	84.42661
River	Kosi	Kosi	Kosi	Narayani	Narayani	Narayani	Narayani
Sampling date	13-Jul-05	10-May-04	10-May-04	12-Aug-07	12-Aug-07	12-Aug-07	12-Aug-07
Type of sediment	Bank	Bank	Bank	Suspended Load	Suspended Load	Suspended Load	Suspended Load
Sampling Depth (m)				0	3.3	6	8
Cs	4.77	11.1	8.43	10.9	10.6	10.3	10.6
Rb	91.8	107	101	146	142	141	142
Ba	294	362	334	460	454	437	441
Th	14.7	19.4	13.6	14.8	15.2	15.8	15.5
U	2.75	3.79	2.60	3.18	4.26	3.33	3.26
Nb	9.21	19.4	13.5	13.6	13.1	12.4	12.6
Ta	1.08	1.75	1.33	1.25	1.33	1.24	1.23
La	32.4	40.9	29.7	32.8	35.8	36.9	35.4
Ce	71.1	97.8	73.5	68.7	73.9	77.1	73.7
Pr	7.59	10.0	7.14	7.43	8.07	8.48	8.06
Pb	15.3	15.7	17.2	24.8	72.0	23.6	24.1
Nd	27.8	36.9	26.7	26.9	29.6	30.9	29.7
Sr	92.6	60.1	67.2	234	213	197	194
Sm	5.43	7.43	5.30	5.26	5.74	6.03	5.82
Zr	159	281	202	217	220	213	200
Hf	3.96	7.57	5.30	5.54	5.63	6.34	5.18
Ti	1903	4248	2884	3021	2916	2710	2777
Eu	0.871	1.24	0.903	0.984	0.973	1.03	0.997
Gd	4.59	6.39	4.59	4.52	4.94	5.05	4.81
Tb	0.724	0.974	0.714	0.712	0.706	0.74	0.734
Dy	4.54	5.93	4.11	4.20	4.40	4.29	4.44
Ho	0.922	1.18	0.815	0.838	0.843	0.815	0.875
Y	27.2	34.9	24.0	25.1	24.0	24.1	25.1
Er	2.76	3.45	2.31	2.47	2.43	2.29	2.52
Li	17.6	40.3	27.1	45.9	43.9	41.2	43.7
Yb	2.65	3.27	2.26	2.36	2.38	2.18	2.34
Lu	0.386	0.476	0.326	0.343	0.35	0.323	0.344
Sc	5.51	9.96	5.14	9.72	9.31	8.90	9.24
V	29.2	78.0	51.8	57.8	55.0	52.0	53.3
Cr	24.8	61.7	37.0	48.0	44.6	41.9	44.0
Co	5.82	13.9	9.26	9.07	8.94	8.28	8.37
Ni	11.9	36.3	20.9	21.5	20.0	18.9	20.1
Cu	9.31	37.6	34.0	17.6	14.7	16.2	14.9
Zn	32.7	77.9	56.5	68.2	64.9	60.8	63.4
As	3.07	11.3	4.04	11.0	11.9	9.86	9.82
wt.%							
SiO2	79.11	61.28	72.72	53.31	56.78	59.47	57.77
Al2O3	9.13	16.30	12.31	11.17	11.34	10.97	11.17
Fe2O3	2.96	5.96	4.11	3.79	3.82	3.60	3.66
MnO	0.06	0.08	0.06	0.05	0.05	0.05	0.05
MgO	1.26	2.46	1.36	2.19	2.07	2.00	2.05
CaO	1.82	2.29	1.39	11.86	10.91	9.38	9.70
Na2O	1.60	1.31	1.58	1.36	1.38	1.47	1.45
K2O	1.95	3.96	2.95	2.78	2.84	2.72	2.78
TiO2	0.34	0.74	0.49	0.49	0.49	0.46	0.47
P2O5	0.13	0.16	0.13	0.11	0.11	0.11	0.11
LOI	1.70	4.93	2.55	11.64	10.10	8.93	9.40
Total	100.05	99.46	99.63	98.74	99.89	99.16	98.60

Sample Name	LO 755 Dup	LO 758 C*	PB 54*	LO 1002	LO 1007	LO 1007 Dup	BR 8106*
Locality	Narayanghat, Nepal	Narayanghat, Nepal	Narayanghat, Nepal	Narayanghat, Nepal	Narayanghat, Nepal	Narayanghat, Nepal	Hajipur, India
Latitude	27.70297	27.70297	27.70297				25.67933
Longitude	84.42661	84.42661	84.42661				85.19362
River	Narayani	Narayani	Narayani	Narayani	Narayani	Narayani	Narayani
Sampling date	12-Aug-07	12-Aug-07	11-Jul-05	16-Jul-10	16-Jul-10	16-Jul-10	17-Aug-08
Type of sediment	Suspended Load	Suspended Load	Suspended Load	Suspended Load	Suspended Load	Suspended Load	Suspended Load
Sampling Depth (m)	8	8.5	8	0	0	0	0
Cs	10.8	5.02	8.5	12.7	3.43	3.14	11.1
Rb	148	85.3	123	170	70.4	62.0	141
Ba	457	290	437	510	307	280	497
Th	14.9	7.87	11.7	14.4	13.4	12.3	17.2
U	3.24	2.02	2.69	3.38	3.33	2.96	3.20
Nb	13.2	6.79	10.7	13.2	14.5	12.9	15.2
Ta	1.30	0.581	1.01	1.18	1.06	0.922	1.28
La	33.2	22.2	28.9	32.1	37.5	34.0	38.3
Ce	69.1	45.8	60.2	66.2	79.9	72.8	81.8
Pr	7.57	4.95	6.7	7.43	8.82	7.99	8.9
Pb	25.0	15.5	19.3	27.4	13.6	12.2	26.7
Nd	27.3	17.8	24.2	27.3	32.9	29.5	32.4
Sr	200	112	177	269	68.9	63.0	159
Sm	5.41	3.41	4.70	5.22	6.22	5.45	6.21
Zr	236	113	188	187	209	190	190
Hf	5.88	2.98	4.83	4.85	5.30	4.74	5.00
Ti	2840	1519	2568	3291	2542	2272	3532
Eu	0.986	0.64	0.894	0.97	1.09	0.98	1.16
Gd	4.68	2.86	4.10	4.34	5.00	4.45	5.34
Tb	0.728	0.423	0.627	0.686	0.774	0.675	0.825
Dy	4.53	2.57	3.87	4.15	4.61	4.23	4.88
Ho	0.913	0.532	0.786	0.819	0.968	0.853	0.966
Y	26.9	15.7	22.6	24.0	28.2	25.3	28.0
Er	2.65	1.61	2.25	2.42	2.83	2.56	2.76
Li	46.7	22.3	32.1	51.6	14.8	13.4	45.3
Yb	2.53	1.56	2.17	2.27	2.79	2.50	2.63
Lu	0.371	0.226	0.307	0.334	0.402	0.363	0.381
Sc	9.38	5.78	8.52	10.5	5.00	5.26	10.6
V	54.9	36.1	51.9	69.4	46.6	41.9	79.9
Cr	45.6	38.3	38.8	58.9	32.0	28.7	59.5
Co	8.55	4.54	7.64	11.2	7.43	6.54	13.4
Ni	20.7	18.7	16.7	28.7	17.8	17.3	32.6
Cu	16.5	11.9	10.1	25.8	25.0	22.2	112
Zn	65.0	37.8	49.7	80.8	42.8	38.2	128
As	9.57	1.68	5.12	14.4	2.84	2.52	12.3
wt.%							
SiO2		69.39	62.71	53.70	75.74		53.31
Al2O3		8.44	10.20	12.22	8.21		14.51
Fe2O3		2.55	3.63	4.60	3.62		5.32
MnO		0.05	0.06	0.06	0.08		0.07
MgO		2.49	2.31	2.50	2.23		2.86
CaO		5.90	8.83	12.36	2.92		8.13
Na2O		1.36	1.45	1.34	1.33		1.23
K2O		1.97	2.61	3.19	1.54		3.57
TiO2		0.28	0.45	0.57	0.44		0.61
P2O5		0.07	0.11	0.13	0.14		0.14
LOI		6.40	8.19		3.73		10.28
Total		98.91	100.55	90.65	99.97		100.03

Sample Name	BR 8107*	MAR-55	MAR-58	MAR-70	MAR-31	MAR-29	MAR-19
Locality	Hajipur, India	Tal, Nepal	Chamje, Nepal	Besi Sahar, Nepal	Philesangu, Nepal	Suribar, Nepal	Turture, Nepal
Latitude	25.67933	28.46715	28.44050	28.23178	28.19050	28.13133	28.03650
Longitude	85.19362	84.37253	84.38800	84.38290	84.41967	84.44050	84.46467
River	Narayani	Marsyandi	Marsyandi	Marsyandi	Marsyandi	Marsyandi	Marsyandi
Sampling date	17-Aug-08	16-Nov-00	16-Nov-00	18-Nov-00	6-Nov-00	6-Nov-00	4-Nov-00
Type of sediment	Bedload	Bedload	Bedload	Bedload	Bedload	Bedload	Bedload
Sampling Depth (m)							
Cs	7.48	17.5	14.4	6.32	5.80	7.30	6.07
Rb	111	194	166	94.6	78	104	84.2
Ba	390	420	283	328	284	331	279
Th	13.6	16.0	16.3	46.3	26.8	8.24	21.0
U	2.39	8.37	5.68	8.87	5.58	5.64	5.12
Nb	9.14	8.99	12.8	26.5	11.5	9.84	11.7
Ta	0.844	0.986	1.79	3.6	1.17	0.865	1.61
La	30.9	37.5	38.1	97.1	68.2	22.2	50.7
Ce	68.6	60.6	79.0	201	134	44.8	104
Pr	7.11	8.85	8.99	22.9	15.4	5.10	11.6
Pb	20.9	29.5	28.4	20.4	17.7	17.1	17.8
Nd	25.5	32.7	33.4	84.5	56.5	18.8	43.6
Sr	128	276	220	120	146	135	133
Sm	4.82	7.63	7.11	16.7	10.9	3.75	8.60
Zr	189	137	160	154	196	123	159
Hf	4.78	3.73	4.41	4.33	5.13	3.32	4.41
Ti	2085	1536	1948	4254	2472	2178	2494
Eu	0.825	1.48	1.04	2.25	1.61	0.771	1.27
Gd	3.93	8.11	6.04	14.1	8.99	3.59	7.34
Tb	0.579	1.57	0.981	2.28	1.31	0.614	1.23
Dy	3.19	10.9	5.41	15.0	7.95	4.63	8.10
Ho	0.605	2.52	1.01	3.13	1.56	1.03	1.79
Y	17.5	77.2	28.3	91.6	44.8	29.5	50.9
Er	1.71	7.94	2.65	9.43	4.64	3.21	5.49
Li	25.1	72.3	52.5	27.0	24.0	30.8	24.6
Yb	1.64	7.58	2.40	9.16	4.54	3.31	5.61
Lu	0.239	1.09	0.336	1.29	0.671	0.481	0.812
Sc	6.21	7.84	5.99	15.3	13.4	10.2	11.4
V	44.6	26.8	29.5	66.7	43.6	49.1	45.0
Cr	41.0	35.1	25.2	53.7	41.6	39.7	36.6
Co	8.39	4.40	6.22	14.9	9.08	8.44	10.6
Ni	22.4	9.98	12.5	24.1	16.5	17.0	15.7
Cu	12.0	5.83	8.38	23.4	11.7	10.9	14.0
Zn	44.4	36.3	41.4	45.7	42.0	46.2	40.2
As	2.75	8.92	23.5	52.6	10.2	3.90	14.2
wt.%							
SiO2	71.09	60.58	61.26	64.74	69.63	70.04	71.31
Al2O3	10.07	11.20	10.64	11.77	10.22	10.42	10.30
Fe2O3	3.22	2.11	2.74	7.68	4.17	4.13	4.81
MnO	0.05		0.03	0.21	0.11	0.09	0.14
MgO	1.54	1.17	1.39	2.12	1.71	1.88	1.61
CaO	4.25	10.68	11.14	5.55	6.51	5.36	5.26
Na2O	1.57	2.35	2.36	1.47	1.66	1.62	1.68
K2O	2.55	3.13	2.74	1.98	1.58	2.03	1.64
TiO2	0.38	0.26	0.34	0.73	0.45	0.36	0.45
P2O5	0.07	0.11	0.15	0.22	0.18	0.11	0.16
LOI	4.19	8.23	7.04	3.37	3.81	3.78	3.10
Total	98.98	99.82	99.83	99.84	100.03	99.82	100.46

Sample Name	MAR-12	MAR-10	MAR-10 Dup
Locality	Anpu, Nepal	Lobrang, Nepal	Lobrang, Nepal
Latitude	27.90783	27.86983	27.86983
Longitude	84.54217	84.55083	84.55083
River	Marsyandi	Marsyandi	Marsyandi
Sampling date	3-Nov-00	3-Nov-00	3-Nov-00
Type of sediment	Bedload	Bedload	Bedload
Sampling Depth (m)			
Cs	8.10	6.85	7.27
Rb	148	106	119
Ba	350	333	366
Th	11.5	10.2	10.7
U	2.87	2.06	2.29
Nb	8.02	8.17	8.85
Ta	0.932	0.738	0.793
La	25.0	27.4	31.8
Ce	49.4	47.6	53.3
Pr	5.41	5.78	6.53
Pb	23.6	18.1	18.9
Nd	20.3	20.9	23.4
Sr	155	146	151
Sm	5.04	4.00	4.22
Zr	141	109	56.0
Hf	3.69	2.95	1.62
Ti	1624	1765	1766
Eu	0.817	0.814	0.857
Gd	6.49	3.57	3.84
Tb	1.68	0.619	0.61
Dy	16.8	4.33	4.13
Ho	4.78	0.907	0.889
Y	137	25.5	25.1
Er	18.2	2.75	2.66
Li	28.9	27.8	27.4
Yb	20.2	2.67	2.62
Lu	2.68	0.382	0.38
Sc	9.45	13.8	10.4
V	34.6	38.4	37.4
Cr	30.6	39.0	34.7
Co	5.40	5.93	5.56
Ni	11.3	11.8	11.5
Cu	6.42	7.37	8.09
Zn	32.6	38.7	37.4
As	5.55	3.34	3.17
wt.%			
SiO2	71.18	71.15	
Al2O3	9.93	9.60	
Fe2O3	2.85	2.91	
MnO	0.05	0.05	
MgO	1.19	1.49	
CaO	5.86	6.04	
Na2O	1.81	1.64	
K2O	2.01	1.87	
TiO2	0.29	0.29	
P2O5	0.11	0.14	
LOI	4.53	4.63	
Total	99.81	99.81	

Supplementary Table C: Trace-element concentrations in rock standards analyzed as unknown samples (ppm)

	BR ref *Chauvel et al. (2011)*	BR 24 ref *Chauvel et al. (2011)*	AGV-1 n=2	2σ (%)	AGV-1 *Chauvel et al. (2011)*	Diff (%)	BEN n=10	2σ (%)	BEN *Chauvel et al. (2011)*	Diff (%)	JSd-2 n=28	2σ (%)	JSd-2 *Chauvel et al. (2011)*	Diff (%)
Li	15.1	7.15	10.8	9.7	10.9	1.1	13.2	4.1	13.0	-1.2	22.8	5.4	22.1	-3.1
Sc	22.8	25.9	12.2	11.1	12.8	4.5	23.0	6.8	22.5	-2.3	17.8	6.2	17.9	0.8
Ti	15300	17500	5955	5.7	6080	2.0	15492	5.2	15400	-0.6	3569	4.0	3570	0.0
V	226	267	115	1.9	117	1.8	229	5.3	226	-1.4	125	4.4	126	0.9
Cr	338	425	7.91	4.5	8.05	1.7	346	5.7	340	-1.6	104	6.5	106	2.0
Co	56.6	52.6	14.9	0.9	15.3	2.3	61.0	5.7	60.0	-1.6	47.6	5.1	47.5	-0.2
Ni	259	238	14.6	2.8	14.5	-0.7	265	6.4	258	-2.8	91.7	6.2	91.1	-0.7
Cu	68.8	37.0	57.1	5.4	57.2	0.2	68.8	8.9	69.3	0.7	1040	9.0	1060	1.9
Zn	158	109	77.4	6.2	91.7	15.6	122	4.8	119	-2.6	1996	17.3	1980	-0.8
As	2.22		1.03	11.6	0.98	-5.1	2.23	37.6	1.80	-24.1	38.3	45.4	37.8	-1.4
Rb	46.6	80.0	68.0	9.5	66.8	-1.8	47.5	6.1	46.8	-1.6	26.3	8.2	25.8	-2.0
Sr	1340	607	662	1.9	657	-0.8	1381	3.5	1380	-0.1	213	7.6	210	-1.4
Y	28.9	28.5	19.4	1.4	19.5	0.6	29.3	4.4	29.0	-1.2	18.4	2.7	18.2	-1.3
Zr	273	294	237	1.0	237	0.2	278	4.4	274	-1.5	108	7.9	103	-4.7
Nb	115	38.1	14.5	0.2	13.9	-4.6	116	5.0	116	-0.2	4.39	8.3	4.19	-4.8
Cs	0.82	0.648	1.29	2.3	1.29	0.3	0.754	6.0	0.752	-0.2	1.07	3.9	1.05	-2.0
Ba	1090	390	1217	2.7	1230	1.0	1055	2.6	1050	-0.5	1264	4.4	1230	-2.7
La	82.6	33.6	38.3	0.5	38.0	-0.9	83.4	2.1	83.0	-0.5	11.3	4.0	10.8	-4.3
Ce	155	73.9	69.7	1.5	69.0	-1.0	157	2.8	155	-1.2	23.5	7.6	22.1	-6.5
Pr	17.4	9.61	8.39	0.5	8.47	0.9	17.6	3.4	17.4	-1.4	3.03	3.6	2.94	-3.0
Nd	66.4	39.9	31.7	0.5	31.8	0.2	67.2	3.1	67.0	-0.3	12.5	3.5	12.1	-3.3
Sm	12.2	8.36	5.75	4.7	5.77	0.3	12.3	3.5	12.2	-0.8	2.95	3.8	2.86	-3.2
Eu	3.66	2.53	1.61	4.2	1.61	0.3	3.67	3.0	3.67	0.0	0.853	5.8	0.872	2.2
Gd	9.88	7.28	4.68	0.0	4.69	0.1	9.83	2.5	9.87	0.5	3.04	3.7	2.85	-6.5
Tb	1.25	1.03	0.611	0.9	0.632	3.4	1.26	3.0	1.26	0.2	0.479	3.6	0.465	-3.0
Dy	6.42	5.77	3.57	5.1	3.55	-0.7	6.52	2.3	6.44	-1.2	3.10	3.3	3.04	-1.8
Ho	1.08	1.05	0.674	2.0	0.675	0.1	1.09	3.2	1.08	-1.1	0.651	2.5	0.641	-1.5
Er	2.58	2.70	1.85	5.6	1.84	-0.5	2.60	4.3	2.59	-0.4	1.95	2.7	1.91	-1.9
Yb	1.84	2.13	1.66	6.6	1.65	-0.8	1.86	3.8	1.84	-1.2	1.94	3.3	1.91	-1.8
Lu	0.246	0.297	0.247	4.6	0.241	-2.6	0.248	5.9	0.245	-1.3	0.293	4.8	0.288	-1.8
Hf	5.67	6.75	5.09	1.1	5.05	-0.8	5.72	3.2	5.64	-1.5	2.72	8.8	2.74	0.7
Ta	5.55	2.34	0.809	1.9	0.825	2.0	5.83	12.7	5.57	-4.6	0.369	17.7	0.345	-7.0
Pb	4.77	3.69	35.2	0.8	35.9	1.9	4.22	8.7	4.17	-1.2	160	7.2	154	-4.2
Th	10.7	4.75	6.37	2.8	6.35	-0.3	10.8	3.0	10.7	-0.9	2.62	3.3	2.43	-8.0
U	2.39	1.20	1.80	4.0	1.83	1.5	2.42	5.1	2.39	-1.1	1.13	10.2	1.09	-4.0

Standard deviations (2σ) were calculated between the n measurement compositions of the rock standards analysed as unknown samples and calibrated to the BR or BR 24 standards using the reference values of Chauvel et al. (2011). Differences between the published values and our measurement compositions (Diff) are also reported.

Supplementary Table D: Present-day ratios used to calculate the present-day compositions of the reservoirs formed at different times in the past

	Nd (ppm)	147Sm/144Nd	143Nd/144Nd	Hf (ppm)	176Lu/177Hf	176Hf/177Hf	Sources in the litterature
CHUR		0.1960	0.512630		0.0336	0.282785	Bouvier et al. (2008)
MORB	12.03	0.2107	0.513074	2.79	0.0383	0.283199	Gale et al. (2013) for Nd and Hf concentrations and for Nd isotopic composition. εHf calculated to be on the present-day Terrestrial Array of Vervoort et al. (2011)
Depleted Mantle	1.2		0.513074	0.3		0.283199	Gale et al. (2013) for Nd isotopic composition. εHf calculated to be on the present-day Terrestrial Array of Vervoort et al. (2011). Nd and Hf concentrations estimated at 10% of the MORB concentrations.
OIB		0.1374	0.512896		0.0082	0.282973	GEOROC database for Nd isotopic composition. εHf calculated to be on the present-day Terrestrial Array of Vervoort et al. (2011).
Oceanic sediment	28.0	0.1314	0.512180	1.78	0.0191	0.282829	Chauvel et al. (2008) for Hf isotopic composition. Plank (2013) for Nd and Hf concentrations and Nd isotopic compositions
Continental Crust		0.1179			0.0115		Rudnick and Gao (2003)

References:

Bouvier A., Vervoort J. D. and Patchett P. J. (2008) The Lu–Hf and Sm–Nd isotopic composition of CHUR: constraints from unequilibrated chondrites and implications for the bulk composition of terrestrial planets. Earth and Planetary Science Letters 273, 48–57.

Chauvel C., Lewin E., Carpentier M., Arndt N. T. and Marini J.-C. (2008) Role of recycled oceanic basalt and sediment in generating the Hf–Nd mantle array. Nature Geosciences 1, 64–67.

Gale A., Dalton C. A., Langmuir C. H., Su Y. and Schilling J.-G. (2013) The mean composition of ocean ridge basalts. Geochem. Geophys. Geosyst. 14, 489–518, doi: 10.1029/2012GC004334.

Plank, T. (2013, in press), The Chemical Composition of Subducting Sediments, in The Crust Vol.3 Treatise on Geochemistry (ed. R. L. Rudnick). Elsevier-Pergamon, Oxford.

Vervoort J., Plank T. and Prytulak J. (2011) The Hf-Nd isotopic composition of marine sediments. Geochimica et Cosmochimica Acta 75, 5903-5926.

Rudnick R. L. and Gao S. (2003) The Composition of the Crust. In The Crust Vol.3 Treatise on Geochemistry (ed. R. L. Rudnick). Elsevier-Pergamon, Oxford. pp. 1–64.